Spatio-temporal patterns and drivers of terrestrial Dissolved Organic Carbon (DOC) leaching to the European river network.

Céline Gommet[1,3], Ronny Lauerwald[2], Philippe Ciais[3], Bertrand Guenet[4], Haicheng Zhang[1], Pierre Regnier[1]

[1]Biogeochemistry and Earth System Modelling, Department of Geoscience, Environment and Society, Universite Libre de Bruxelles, Bruxelles, Belgium
[2]Université Paris-Saclay, INRAE, AgroParisTech, UMR ECOSYS, 78850, Thiverval-Grignon, France
[3]Laboratoire des Sciences du Climat et de l'Environnement, UMR8212, CEA-CNRS-UVSQ F-91191 Gif sur Yvette, France
[4]Laboratoire de Géologie, UMR 8538, Ecole Normale Supérieure, IPSL, PSL Research University, CNRS, Paris, France

Correspondence to: Céline Gommet (celine.gommet@ulb.be)

Abstract. Leaching of dissolved organic carbon (DOC) from soils to the river network is an important component of the land carbon (C) budget. At regional to global scales, its significance has been estimated through simple mass budgets, often using multi-year averages of observed fluvial DOC fluxes as proxy of DOC leaching due to the limited availability of observations of the leaching flux itself. This procedure leads to a systematic underestimation of the leaching flux because of the reactivity of DOC during fluvial transport. Moreover, this procedure does not allow to reveal spatio-temporal variability in DOC leaching from soils, which is needed to better understand the drivers of DOC leaching and its impact on the local soil C budget. In this study, we use the land surface model ORCHILEAK to simulate the terrestrial C budget including leaching of DOC from the soil and its subsequent reactive transport through the river network of Europe. The model performance is not only evaluated against the sparse observations of DOC leaching, but also against the more abundant observations of fluxes and reactivity of DOC in rivers, providing further evidence that our simulated DOC leaching fluxes are realistic. The model is then used to simulate the spatio-temporal patterns of DOC leaching across Europe over the period 1972 to 2012, quantifying both the environmental drivers of these patterns as well as the impact of DOC leaching on the land C budget. Over the simulation period, we find that on average 14.3 TgC yr^{-1} of DOC is leached from land to European rivers, which is only about 0.6% of the terrestrial net primary production, a fraction about one order of magnitude lower than reported for tropical river networks. Of the DOC leaching, on average 12.3 TgC yr^{-1} is exported to the coast via the river network, the rest being respired in transit. DOC leaching presents a large seasonal variability, with a maximum occurring in winter and a minimum in summer, except for the Northern most part of Europe where the maximum occurs in spring due to the snow melt. DOC leaching rate is generally lower in warm and dry regions, and higher in cold and wet regions of Europe. Furthermore, runoff, and the ratio between runoff from shallower flow paths vs. deep drainage and groundwater flow, is the main driver of the spatial variation of DOC leaching. Temperature, as a major control of DOC production and decomposition rates in the soils, plays only a secondary role.

1 Introduction

38

39 Land ecosystems are an important carbon (C) sink which absorbs about one fourth of anthropogenic CO_2

40 emissions and stores it in increasing biomass and soil carbon pools (Friedlingstein et al., 2020). This terrestrial

41 sink mitigates the growth rate of atmospheric CO_2 and thus plays an important role in regulating climate change

42 (Ciais et al., 2013). However, the efficiency of that sink is partly alleviated by the permanent, lateral leaching of

43 C from soils, through the river network down to the ocean (Regnier et al., 2013). An accurate understanding of

44 lateral carbon fluxes through the river network is thus necessary to better understand the global C cycle and to

45 inform policies of climate change mitigation (Le Quéré et al., 2018).

46 The identification of riverine C transfers as a key component of the continental C budget constituted an

47 important paradigm shift in our understanding of the global C cycle (Cole et al., 2007). More recently, riverine C

48 cycling was also shown to be affected by anthropogenic perturbation and thus to be an element of the

49 anthropogenic CO_2 budget (Regnier et al., 2013; Le Quéré et al. 2015). Anthropogenic perturbations of riverine

50 C fluxes are manifold and comprise direct impacts through changing C and nutrient inputs following land-use

51 change and agricultural activities, wastewater discharge, and hydraulic management (e.g. Tian et al., 2015;

52 Lauerwald et al., 2020; Hastie et al., 2021; Maavara et al., 2017). There are also indirect impacts following

53 climate change and changes in atmospheric composition. Together, these perturbations have accelerated the

54 turnover of C along the terrestrial-inland water continuum. The terrestrial C sink, which is classically estimated

55 without taking into account the C exports through the river network, is thus generally overestimated (Regnier et

56 al., 2013; Lauerwald et al., 2020).

57 The integration of riverine C transfers into the terrestrial C budget requires the quantification of the amount of C

58 lost from soils to the river network. Due to the scarcity of observational data, this flux is not easy to determine

59 based on empirical methods. At global scale, this flux was estimated through budget closure based on estimates

60 of riverine C exports to the coast and estimates of C losses to the atmosphere and aquatic sediments during

61 transport. The existing global estimates of these soil C exports to the river network, as synthesized by Drake et

62 al. (2018), range from 1.1 to 5.1 PgC yr^{-1} – a huge uncertainty range reflecting the limitations of empirical

63 estimation approaches and the paucity of underlying data. Over the past decade, a new generation of land surface

64 models (LSMs) have been developed, which represent the export of C from soils to the river network, and in

65 some cases even the transport and cycling of these terrestrial C loads along the river network down to the coast

66 (Smith et al. 2010; Kicklighter et al. 2013; Tian et al., 2015; Lauerwald et al., 2017; Nakhavali et al., 2018).

67 With the exception of the study by Tian et al. 2015, all these studies focus on the lateral export of dissolved

68 organic C (DOC) which is a product of the incomplete decomposition of plant litter and soil organic carbon

69 (SOC). These mechanistically based models allow to predict the leaching of DOC in unmonitored regions and to

70 assess the spatial and temporal variability which, to date, can only be poorly resolved by empirical methods.

71 Moreover, these approaches link the C exports from soils to the river network to the terrestrial C cycle, and thus

72 allow to directly assess the role of these C exports in the terrestrial C budget, its perturbation through land use,

73 land use change and changes in climate and atmospheric chemistry, and its impact on the terrestrial sink for

74 anthropogenic CO_2 emissions.

75 In this study, we use the LSM ORCHILEAK (Lauerwald et al. 2017), a branch of the IPSL-LSCE LSM
76 ORCHIDEE (Krinner et al. 2005), to quantify the DOC leaching from soils and its effects on the terrestrial C
77 budget in Europe. ORCHILEAK not only simulates the vertical C cycling between vegetation, soils and
78 atmosphere in response to climate, atmospheric CO_2 concentrations, and land use change, but also represents the
79 lateral exports of DOC from soils to the river network as well as the reactive transport of that DOC through the
80 river network. To our knowledge, only one study (Kindler et al., 2011) estimated the soil DOC leaching flux
81 based on runoff and direct observations of DOC concentrations in the soil water for various locations across
82 Europe, and will thus be used for direct evaluation of the simulated leaching fluxes. Further, we evaluate
83 simulated against observed riverine DOC fluxes which are available from different water quality surveys and
84 scientific publications. Assuming a realistic representation of DOC reactivity in the river network, which is to be
85 evaluated against observations as well, this model-data comparison of riverine DOC fluxes represents a valuable,
86 additional possibility to assess the validity of simulated soil DOC leaching.

87 So far, ORCHILEAK has been successfully tested and applied on large, near-natural river systems such as the
88 Amazon (Lauerwald et al. 2017, Hastie et al. 2019, Lauerwald et al. 2020), the Congo (Hastie et al. 2021) and
89 the Lena Rivers with a version also including some specific permafrost related mechanisms (Bowring et al.
90 2019, 2020). In this study, for the first time, ORCHILEAK is applied to, and evaluated for, the European river
91 network which is subject to direct impacts of agricultural land use, in contrast to more natural river basins. For
92 this reason, we devote special attention to manure application as an anthropogenic non-point source of DOC to
93 the river network, while we assume that for the period of simulation (1979-2012), due to quality of sewage water
94 treatment, anthropogenic point sources of DOC are now negligible for most parts of Europe.

95 Making full use of the capabilities of the ORCHILEAK model, we study in detail the spatio-temporal patterns in
96 DOC leaching and its quantitative contribution to the terrestrial C budget across Europe. We investigate how
97 specific climate zones in Europe differ with regard to seasonality in DOC leaching fluxes, which are
98 hypothesized to be controlled by hydrology, litter fall and temperature effects on litter and SOC decomposition.
99 We will further try to quantify the effect of these controls in the different climate zones of Europe. Finally, we
100 strive to find out in which climate zone DOC leaching affects the terrestrial C budget the most.

2 Methodology

2.1 ORCHILEAK

2.1.1 Model overview

ORCHILEAK (Lauerwald et al., 2017) is a branch of the model ORCHIDEE (Organizing Carbon and Hydrology in Dynamic Ecosystems) (Krinner et al., 2005), the land surface component of the Institut Pierre-Simon Laplace (IPSL) Earth system model (ESM). ORCHIDEE simulates energy, water and C fluxes between the atmosphere and the land at a global scale. This LSM is based on four sub-modules. The first one, SECHIBA, simulates the energy budget (energy, carbon and water) between the atmosphere and the biosphere as well as the hydrology, which in the default set-up used here, are both represented using a 30 minute time-step. The second sub-module, adapted from the LPJ model (Sitch et al., 2003), represents the dynamics of vegetation distribution on long time scales (1 year), while the third one (STOMATE) simulates the C dynamics in vegetation and soils at a daily to sub-daily step (Krinner et al., 2005). Finally, the fourth sub-module handles the routing of water that is lost via surface runoff and drainage from soils to the ocean through the global river network (Polcher 2003, Guimberteau et al.,2012), for which a daily time-step is used. All processes are simulated on a horizontal model grid, the resolution of which can be adapted to that of the meteorological forcing files. In this study, simulations are run at a spatial resolution of 0.5°. Moreover, in the default set-up, up to 13 plant function types (PFTs; bare soil, eight types of forest, two types of grassland and two types of cropland) can be distinguished for each cell, for which C budgets are simulated individually, while energy and water budgets are simulated at the grid cell level.

ORCHIDEE represents the soil C dynamics distinguishing different pools of plant litter and soil organic C over a 2 m profile. A branch of ORCHIDEE, called ORCHIDEE-SOM (Camino et al. 2018), added a vertical discretization of these carbon pools over 11 layers and included the representation of DOC production and cycling within the soil column (see section 2.1.2 for more details). ORCHILEAK was built on this branch and accounts for the coupled reactive transport processes impacting the dissolved C inputs from soils to the river network, including both DOC leaching from soils and CO_2 produced by soil respiration, into the hydrologic routing scheme. Besides advective transport of carbon with the water flow, ORCHILEAK simulates the decomposition of DOC during riverine transport, the gas exchange of CO_2 at the interface between the inland water and the atmosphere, and the exchange of C between water column and soil column in inundated floodplains. All those fluxes are closely coupled to the model representation of hydrology that comprises interception of precipitation, throughfall, infiltration, percolation, surface runoff, drainage, and the routing of discharge along the river-floodplain network.

2.1.2 Soil carbon module

The soil carbon module of ORCHILEAK (Fig. 1) is derived from the CENTURY soil carbon model of Parton et al. (1988). In the standard scheme (Krinner et al., 2005), C in the soil of each model grid cell, and for each PFT,

136   is represented by four different litter and three different soil organic carbon (SOC) pools with different turnover

137   rates. The four litter pools correspond to metabolic aboveground and belowground litter, structural aboveground

138   and belowground litter (Fig. 1). The SOC is subdivided into active, slow and passive pools. In the CENTURY

139   scheme, C from the decomposed structural litter enters the active and the slow pools with the fraction allocated

140   to each pools depending on lignin content of the litter, while the entire metabolic litter pool and the remaining

141   part of structural litter is allocated to the active SOC pool. The SOC pools then feed into each other with the

142   main C flux going from active to slow and passive to represent microbial decomposition of detrital organic

143   matter, and a small return flux of slow and passive C back to the active pool to represent implicitly the C supply

144   in the form of dead microbial biomass.
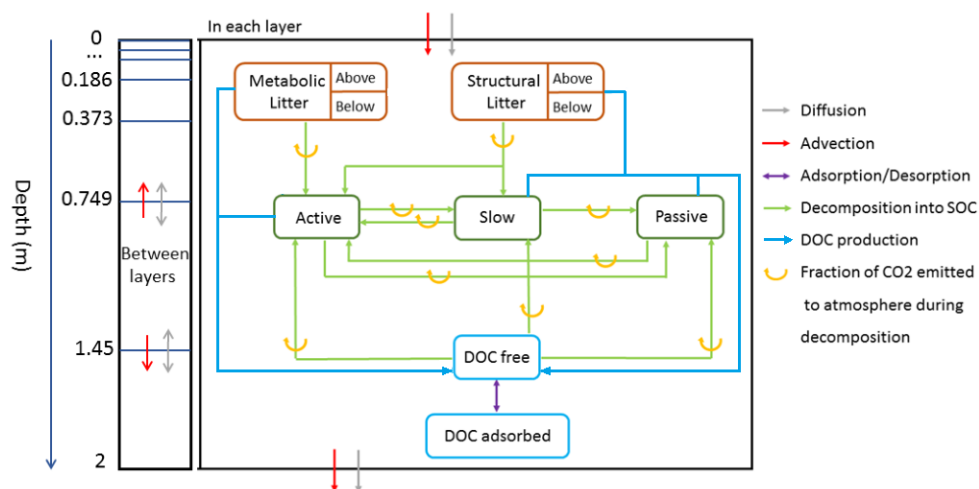
145
146
147   **Figure 1. The new version of the soil module of ORCHIDEE-SOM. The left box represents the discretization of the**
148   **soil column and the transport processes between layers. The right box is a zoom of all the biogeochemical**
149   **transformation processes that occur in each layer.**

150

151   Campoy et al. (2013) updated this scheme with a vertical discretization of distinct SOC and litter pools over a 2

152   m soil profile represented by 11 layers. Camino et al. (2018) further developed the soil C module by including

153   an explicit representation of the fate of DOC along this vertically discretized soil profile. Processes accounted for

154   are DOC production from the decomposition of SOC and litter, decomposition of DOC within the soil,

155   sorption/desorption of DOC onto/from mineral surfaces, vertical advection and diffusion of DOC through the

156   soil column, and lateral, advective leaching of DOC out of the soil profile, along with surface runoff and

157   drainage.

158   The DOC dynamics in the soil is controlled by production, decomposition and transport along the discretized 2

159   m soil column (equation 1):

$$\frac{dDOC_i}{dt} = \sum (Production_i - Decomposition_i) + F_{A,i} + F_{D,i} \qquad (1)$$

160   Where i stand for the index of each layer. Each layer is connected to the adjacent layers by advection F_A and

161   diffusion F_D. The total DOC transport flux is made of an advective component (equation 2) computed as the

162   product of the water flux Q and the DOC concentration (in the i-th layer) and a diffusive component that follows

163   Fick's first law (equation 3):

$$F_A = Q * DOC_i \qquad (2)$$

$$F_D = -D * \frac{\partial^2 DOC}{\partial z^2} \qquad (3)$$

164   where i stands for the ith layer, z for the depth along the discretized soil profile, and D stands for the molecular

165   diffusion coefficient of DOC.

166   The advective export of DOC to the river network is proportional to the top (first five layers, 4.5 cm) and bottom

167   (11th layer) DOC concentrations, corresponding to water loss fluxes associated to runoff (for near surface) and

168   drainage (for deep). We also apply a Fickian-type transport to represent the effect of bioturbation on DOC

169   profiles, as well as on the solid phase SOC and litter profiles. Therefore, in contrast to advection, which only

170   affects DOC entrained with water losses, bioturbation transports both SOC and DOC across the different layers.

171   In addition, DOC is diffusing along the concentration gradient within the soil solution.

172   The right hand-side of Fig. 1 summarizes the set of production/decomposition processes that occur in each layer.

173   During litter decomposition, a fraction of the C is directly emitted back to the atmosphere as CO_2 while the

174   remainder feeds the active and slow SOC pools:

175

$$CO_2\ respiration(Litter) = (1 - CUE) * k_L * (1 - \omega_L) * Litter \qquad (4)$$

$$Litter\ decomposition = CUE * k_L * (1 - \omega_L) * Litter \qquad (5)$$

176   where k_L is the kinetic constant for the litter decomposition (dependent on soil moisture and temperature

177   (Camino et al., 2018)) and ω_L the fraction of litter that is channelled into DOC production (as opposed to

178   particulate soil carbon SOC). This approach of relating DOC production directly to the decomposing litter is

179   inspired by Nakhavali et al., 2018 (following from the ECOSSE model (Smith et al., 2010)) and is a major

180   modification compared to the previous version of soil DOC and POC cycling from Camino et al., 2018. In

181   equations (4) and (5), the partitioning between SOC production and respiration is defined by the carbon use

182   efficiency (CUE).

183   In turn, active SOC is degraded into both slow and passive SOC and the respiration fluxes associated with these

184   processes are also controlled by the CUE (equations 6 and 7, with k_{SOC} as the kinetic constant for SOC

185   decomposition) and ω_{SOC} as the fraction of SOC that is transformed into DOC):

$$CO_2\ respiration(SOC) = (1 - CUE) * k_{SOC} * (1 - \omega_{SOC}) * SOC \tag{6}$$

$$SOC\ decomposition = CUE * k_{SOC} * (1 - \omega_{SOC}) * SOC \tag{7}$$

186

187   The decomposition of the litter and SOC pools produces a small amount of DOC according to equation 8. The

188   DOC pool is thus fed by seven contributing sources, one for each of the four decomposing litter pools and three

189   from the decomposing SOC pools:

190

$$DOC\ production = k_L * \omega_L * Litter + k_{SOC} * \omega_{SOC} * SOC \tag{8}$$

191   In ORCHIDEE-SOM (Camino et al. 2018), all decomposed litter and SOC which is not respired to CO_2, was

192   first fed into the DOC pools, and only upon the decomposition of that DOC, the non-respired fraction of the

193   decomposed DOC could feed the other SOC pools. Such formulation is in contrast to the adaption of the RothC

194   SOC model in ECOSSE (Smith et al., 2010) and JULES (Nakhavali et al., 2018) that we followed here, where

195   the major exchange of C is between the different litter and SOC pools, and the production of DOC is related to

196   these SOC and litter pools by empirical rate constants, which were fitted to reproduce observed DOC turnover

197   times (Kalbitz et al.,2003, Turgeon, 2008) and DOC concentrations in the soil. The much higher DOC

198   production rates simulated by ORCHIDEE-SOM in its original configuration during preliminary tests over

199   Europe led us to implement the new approach (equations 4-7). While preserving the basic structure of

200   ORCHIDEE-SOM, we thus adapted the model in a way that organic C exchange occurs mainly among the

201   particulate litter and SOC pools, similar to the original Century model, while the production of DOC is

202   dependent on leaching rates as used in ECOSSE. In the modified soil carbon module, we used the parameter ω in

203   Equations (4-7) as a scaling factor that determines how much DOC is produced by the decomposition of litter

204   and SOC. This parameter was calculated after Smith et al. (2010) as the ratio of production of DOC from litter

205   (p_{DOC_L}) and the SOC pools ($p_{DOC_{SOC}}$) to the decomposition rates of litter (k_L) and SOC (k_{SOC}). The initial values

206   for ω were 0.5 % and 3 % for the litter and SOC pools, respectively. Further optimization with regard to

207   reproducing observed soil DOC concentrations led to ω values set at 0.2% for the litter and 1.2% for the SOC

208   pools.

209   Once produced, DOC can then adsorb on particles, and desorb from the adsorbed pool back into free DOC pool

210   following an equilibrium reaction between the dissolved and adsorbed phases. The partitioning is controlled by

211   K_D, the so-called equilibrium partition coefficient (equation 9).

212

$$DOC_{adsorption-desorption\ eq} = K_D * DOC \tag{9}$$

213   Finally, the DOC pool is subject to decomposition according to equation (10) and then partly feeds into the SOC

214   pools (eq. 11).

215

$$CO_2\ respiration(DOC) = (1 - CUE) * k_{DOC} * DOC \quad\quad (10)$$

$$SOC\ production\ by\ DOC = CUE * k_{DOC} * DOC \quad\quad (11)$$

216 **2.1.3 Manure as an additional C source**

217 In Europe, a large fraction of the landscape is dominated by agricultural and grazing activities and manure

218 application represents a significant additional C - in particular DOC- source to the soil in regions dominated by

219 grasslands and croplands. To constrain the C flux from manure infiltrating into the soil, we used the gridded $0.5°$

220 resolution input of manure nitrogen (manure-N) applications produced by Zhang et al. (2017) as forcing file.

221 Following the use of that forcing data in the model branch ORCHIDEE-CNP developed by Sun et al. (2021), we

222 assumed that 90% of the total manure-N is in mineral form (i.e. NH_4^+ or NO_3^-) and the remaining 10% is in

223 organic form. To convert the organic manure-N into a manure-C flux, a C:N stochimetric ratio of 13.7 was then

224 applied (Vuichard et al., 2018). Finally, the particulate and dissolved organic manure-C were assumed to feed

225 the litter and DOC pools, respectively (Fig. S1). Consistent with ORCHIDEE-CNP (Goll et al., 2017), the

226 fractions of particulate and dissolved manure-C were set to 0.9 and 0.1, respectively.

227

228 **2.1.4 Hydrological processes**

229 The representation of hydrological processes is handled in two distinct sub-modules. The first one, the hydrology

230 sub-module, simulates the vertical exchange of water in the atmosphere-vegetation-soil system in each model

231 grid cell, while the second one, the river routing module, simulates the horizontal transfers between grid cells.

232 The hydrology is forced by several meteorological fields such as precipitation and air temperature. In the

233 hydrology module, precipitation is divided into interception and throughfall, the latter being further subdivided

234 into surface runoff and infiltration into the soil. The infiltration rate is controlled by the throughfall rate, the

235 slope of the soil surface and the hydraulic conductivity of the soil which is a limiting factor for infiltration. The

236 distribution of water within the soil is represented by the distribution of soil moisture over the discretized soil

237 profile (de Rosnay et al., 2002, d'Orgeval et al., 2008). The water budget within the soil is thus determined by

238 the infiltration rate, the evaporation and transpiration from the soil, and drainage at the bottom of the soil

239 column. The infiltration rate and percolation through the soil profile are then used to compute the advective flux

240 of DOC (equation 2)

241 The second module deals with river routing and represents the horizontal transfers of water from the soil column

242 to the aquatic system though surface runoff and drainage, and further through the river network and adjacent

243 floodplains (Vorosmarty et al., 2000). Note that ORCHILEAK simulates the occasional inundation in the river's

244 floodplains, where decomposition rates of the different carbon pools (litter, SOC and DOC) differ depending on

245 whether the soil is flooded or not. For a detailed description of its features, please refer to Lauerwald et al.

246 (2017).

247

2.2 Simulations

2.2.1 Model set-up

Model domain, land cover and forcing data. The simulated model domain extends over the area covered by the EU-27 (4.1 10^6 km^2) between 35°N and 70°N latitude and 10°W and 30°E longitude (Fig. 2). This domain includes 5600 model grid cells at 0.5x0.5° resolution and encompasses 6 broad climate zones according to the Köppen-Geiger classification from Peel et al., 2017 (Fig. 2a). The dominant PFTs within Europe include croplands (20% mainly C3), grasslands (31% of which 24% are C3), and forests (25% of boreal forest, of which 16% are needleleaved evergreen and 9% are broadleaved summer-green, and 14% of temperate forest, of which 8% are broadleaved summer-green, 3% are needleleaved and 3 % are broadleaved evergreen) (Fig.2b). The spatial distribution of manure application on grasslands and croplands is shown in Fig.2c. Finally, Fig.2d illustrates the actual river network derived from the HydroSHEDS DEM data (Lehner et al., 2008) and the one corresponding to our river routing scheme at 0.5 degree resolution, highlighting that the representation of the river network is not optimal due to the coarse spatial resolution of our model. This coarse resolution limits the possibility of model validation to the downstream parts of larger river networks. Note further that the mouth of the Rhine is more than 100 km too far east, which further limits model validation for that river.
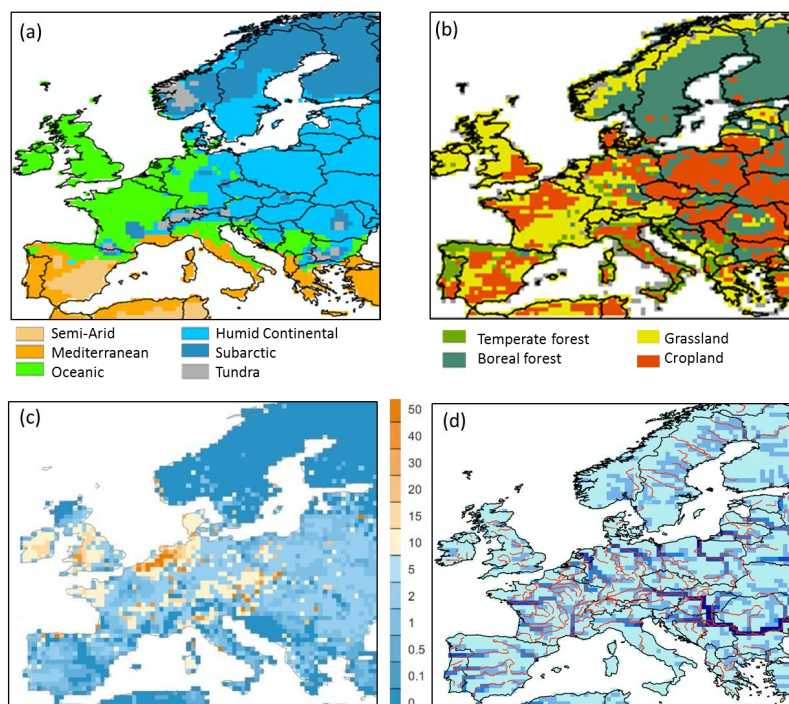
Figure 2. Spatial distribution for each 0.5° grid cell of the continental European domain of (a) climate zones (according to the Koppen-Geiger classification); (b) dominant plant functional types (pft) (c) manure application

266   **(in gC m^{-2} yr^{-1}); (d) the routing Network of ORCHILEAK (in blue). The real river network extracted from the**

267   **European Environment Agency (https://www.eea.europa.eu/legal/copyright) is also shown.**

268

269   The forcing data applied in our study are listed in table 1. They are the same as those used in Lauerwald et al.

270   (2017) except for the meteorological forcing data and the land cover. The WFDEI meteorological forcing dataset

271   used in this study was derived by applying the methodology originally used to create the WATCH Forcing Data

272   (WFD) from the ERA-Interim reanalysis data (Weedon et al., 2014). The dataset has a 0.5° spatial resolution and

273   a 3-hourly time step from 1978 to 2014. The land cover forcing data set, which gives the areal proportion of the

274   13 PFTs within each 0.5° grid cell, was taken from Peng et al. (2017).

275

276   **Table 1. List of the forcing files used for our simulations, along with their spatiotemporal resolution.**

VARIABLE	SPATIAL RESOLUTION	TEMPORAL RESOLUTION	DATA SOURCE
Rainfall, snowfall, incoming shortwave and longwave radiation, air temperature, relative humidity and air pressure, wind speed.	0.5°	3 hours	WFDEI_GPCC (WATCH Forcing Data (WFD) by making use of the ERA-Interim reanalysis data, Global Precipitation Climatology Centre; Weedon et al. (2014))
Soil texture class	0.5°	-	Reynolds et al., 1999
Soil pH, soil bulk density, poor soil	0.5°	-	After HSWD v 1.1 (Fao et al., 2009)
Stream flow directions and topographic index	0.5°	-	STN-30p (Vörösmarty et al., 2000)
Floodplains and swamps	0.5°	-	Guimberteau et al., 2012
River surface area	0.5°	-	Lauerwald et al., 2015
10th, 50th, 90th percentile of the stream reservoir	1°	-	Derived from pre-runs with ORCHIDEE
Land cover	0.5°	-	Peng et al. (2017)

277

278   **Parametrization of hydrological processes**. ORCHILEAK was previously parametrized and validated for the

279   Amazon (Lauerwald et al., 2017; Hastie et al., 2019; Lauerwald et al., 2020), Congo (Hastie et al., 2021) and

280   Lena (Bowring et al., 2020) basins. In our study of the European river network, we used the default parameter

281   values of Lauerwald et al. (2017) excepted for the surface roughness of the vegetation that was adjusted. This

282   parameter increases the aerodynamic resistance near the surface when vegetation cover is low, leading to lower

283   ground temperatures and thus lower evaporation rates. This adjustment was deemed necessary in order to better

284   capture the observed mean and seasonal variability of the discharge along the European river network.

285   **Spin-up.** Before the model can be used to simulate C dynamics over the past decades, a spin up is needed to

286   reach an assumed steady state for the C fluxes during the pre-industrial period. This steady state is achieved by

287   spinning up ORCHILEAK for 15000 years. The spin up was realized by recursively looping over 27 years of

288   climate forcing using the WFDEI forcing dataset over the 1980-2006 period and constant land cover and

289   atmospheric CO_2 concentration of 286 ppm (Guimberteau et al., 2018) corresponding to year 1861. After the end

290   of the spin-up, the soil C stock across the entire European continent changed by less than 1% over a century of

291   simulation, which we considered close enough to steady-state.

292   **Transient runs.** Using the steady-state outputs as initial condition, the first part of the transient simulation

293   (1861-1977) was carried out with increasing atmospheric CO_2 concentration, changing land use and land cover

294   and with river routing activated while still looping over the same 27 years of climate forcing used for the spin-up

295   because no climate forcing data prior to 1978 was available. From then onwards, the WFDEI atmospheric

296   forcing data was applied over the entire period covered by this product (1978-2014).

297

2.2.2 Model evaluation

299   Firstly, the simulated discharges were compared to times series of daily stream flow recorded at eleven gauging

300   stations from "The Global Runoff Data Center (GRDC), 56068 Koblenz, Germany" dataset. For comparison,

301   both observed and simulated discharges were aggregated at the monthly temporal resolution over the years 1980

302   to 2006. This period was chosen based on the GRDC data coverage. Model performance was then evaluated

303   with respect to several variables of the terrestrial C cycle. Firstly, simulated Net Primary Production (NPP) was

304   compared to two different data products. The first one, the CARbon DAta MOdel fraMework (CARDAMOM;

305   Bloom et al., 2015) built from model data fusion analysis at 1° resolution. The second one is the Global

306   Inventory Modeling and Mapping Studies (GIMMS) at 0.5° resolution based on AVHRR and MODIS sensors.

307   GIMMS uses several atmospheric forcing data set to derive NPP. Those are CRUNCEP version 4 P1 and P2

308   (Rainfall, cloudiness, relative humidity and temperature taken from the CRU (Climate Research Unit), while the

309   other fields such as air pressure, longwave radiation, wind speed are directly derived from NCEP (National

310   Center for Atmospheric Research)), ECMWF (European Centre for Medium-Range Weather Forecasts),

311   MERRA2 (the Modern-Era Retrospective analysis for Research and Applications, Version 2) and NCEPR2

312   (https://www.esrl.noaa.gov/psd/). For our comparison, we calculated the average of the NPP obtained with these

313   five atmospheric forcing files. The NPP values from ORCHILEAK and GIMMS were averaged over the period

314   1982-2006 while CARDAMOM only covers a shorter time period comprised between 2001 and 2010. Modeled

315   NPP was then compared to the NPP data products at the European scale and at the scale of five large European

316   basins for which we also evaluated the simulated river discharge and DOC fluxes, and which taken together,

317   represent 19 % of the model domain (Fig.3): the Danube, Rhine, Elbe, Rhone and Seine. All five basins are

318   located in an oceanic or humid continental climate (Fig.2a) although the Rhone basin extends further into the

319   Mediterranean climate zone. The basin characteristics according to land cover types are as follows: the Danube

320 and the Elbe basins have both a high proportion of croplands (around 40%), the remainder being mostly covered

321 by grasslands and boreal forests. The Rhone is covered by 50% of grasslands, while in the Seine basin croplands

322 reach 50%. The Rhine has a more diverse land cover with a substantial proportion (about 30%) of boreal (10 %)

323 and temperate (20 %) forests, 35% of grasslands and 25% of croplands. See table S2 for further details.
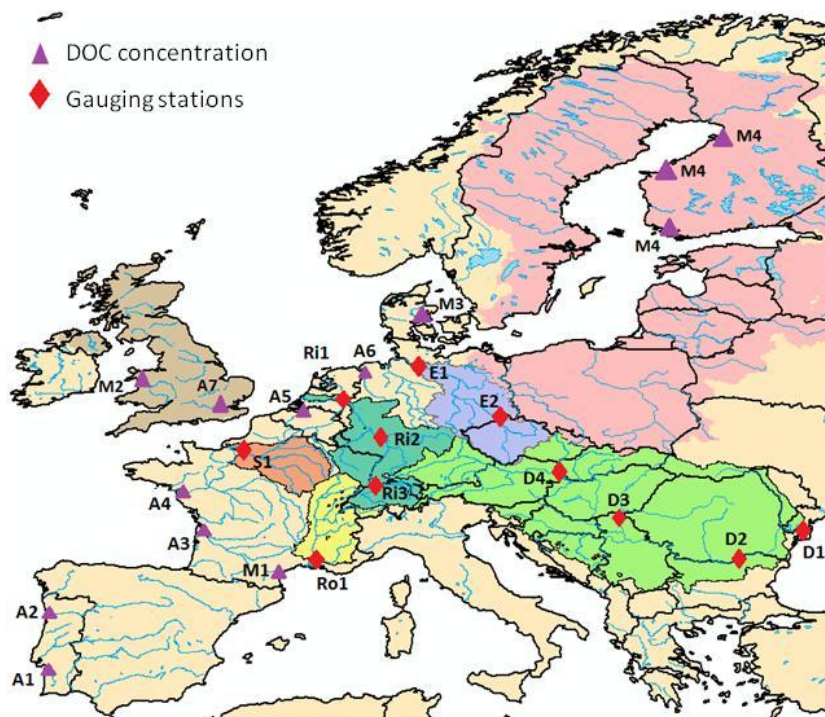
324

325 **Figure 3. Map of continental Europe delineating the (group of) catchments of focus in this study and the location of**
326 **observed discharge and DOC concentrations. Catchments, from west to east are: All UK (light brown), Seine**
327 **(orange), Rhone (yellow), Rhine (dark green), Elbe (violet), All Baltic (pink) and Danube (light green). Observations**
328 **include GRDC stations (red diamonds) in the Seine (S1-Poses), Rhone (Ro1-Beaucaire), Rhine (Ri1-Lobith, Ri2-Main**
329 **in Frankfurt, Ri3-Basel), and Danube (D1-Ceatal Izmael, D2-Svistov, D3-Tisza in Senta, D4-Bratislava) catchments,**
330 **as well as river stations where DOC concentrations were measured (purple triangles): A1-Douro, A2-Sado, A3-**
331 **Gironde, A4-Loire, A5-Scheldt, A6-Ems, A7- Wales, A8-Thames, M1-Tech, M2-Wales, M3-Denmark, M4-Finland**
332 **(Abril et al 2002, Mattsson et al., 2008).**

333

334 SOC from the Harmonized World Soil Database (HWSD) was used to evaluate the simulated SOC stocks

335 against observation-based products. HWSD is a global soil database framed within a Geographic Information

336 System (GIS) that contains up-to-date information on world soil properties. In particular, this dataset reports the

337 organic carbon content in the soil as well as the soil bulk density. The bulk density was calculated in two

338 different ways. The first one follows the method described in Saxton (1986) where the bulk density is related to

339 the soil texture, this approach tending to overestimate density in high porosity soils or in OC rich soils. The

340 second method uses the SOTWIS database in which the bulk density is calculated as a function of soil type and

341   depth. In this database, all variables are reported for the topsoil (0-30cm) and the sub-soil (30-100cm) horizons.

342   For comparison purposes, our simulated SOC stocks were thus integrated over the same depth intervals. We also

343   assessed briefly the extent to which our model can reproduce the main features in observed soil DOC profiles.

344   To that end, we compared our simulated DOC profile averaged over the entire European forest biome against the

345   one established by Camino et al. (2014) on the basis of a synthesis of local measurements. Unfortunately, similar

346   synthetic profiles based on observations have not been constructed for croplands and grasslands.

347   The key variables of interest in our study are the DOC leaching flux from the soil and the DOC export flux to the

348   coast. These fluxes require accurate simulation of the water discharge fed by runoff and drainage as well as of

349   DOC concentrations in the leaching flux and in the riverine flux. For the leaching flux, our simulation results

350   were compared to measured fluxes reported by Kindler et al. (2011) across different locations. Because the

351   observed DOC leaching fluxes reported by Kindler et al. (2011) are based on local measurements that are not

352   easily comparable to simulated fluxes at the coarse spatial resolution of our model (0.5° or about $2*10^3$ km² at

353   the corresponding latitude), we nevertheless consider the comparison against measured river DOC fluxes more

354   relevant for our purpose, as rivers are good integrators of mean, larger-scale catchment properties. For the

355   riverine export fluxes, we assessed the modeled discharges and DOC concentrations separately. For evaluation

356   of stream DOC concentrations, DOC data were extracted from the GLObal RIver CHemistry database

357   (GLORICH, Hartmann et al., 2014) for the Rhine and Elbe basins and from the "Eau de France" database for the

358   Seine and Rhone basins. These data were complemented by river DOC concentrations reported by Abril et al.

359   (2002) for 9 river mouths (Sado, Thames, Ems, Scheldt, Gironde, Douro, Loire, Elbe and Rhine), and by

360   Mattsson et al. (2008) for several river basins located in Finland, Denmark, Wales and France.

361

362   **3 Results and discussion**

363   **3.1 Model evaluation at pan-European and catchment scales**

364   **3.1.1 Discharge**

365   Figure 4 compares the simulated discharge against observations for selected stream gauging stations (section 2).

366   Those stations are located near the mouth of large rivers (Danube, Rhine, Rhone, Elbe and Seine) but also

367   include a few locations further upstream the same rivers or at major tributaries (Fig.3). The comparison is

368   performed for the period 1990-2000, except for the Rhone at Beaucaire and the Danube at Svistov for which the

369   observed stream gauge data cover only a shorter period. Overall, the model reproduces the observations well,

370   both in terms of amplitude and seasonality, except for the Elbe at Neu Darchau for which the temporal variability

371   is well captured but the absolute discharge is overestimated.

372   Note that the simulated catchment area often diverges (by -25% to +30 %) from the observed value due to the

373   coarse resolution (0.5°x0.5°) of ORCHILEAK (Table S3). As a result of the model resolution, smaller tributaries

374   are not represented individually and each grid cell was fully assigned to one larger river basin. The effect of the

375   resolution is also shown in Fig.2d which compared the observed and modeled river network. Discrepancies

376   between model and real world catchment area will translate into proportional biases in discharge simulation.

377   Furthermore the 0.5° resolution is too coarse to be able to represent perfectly the pathways of the river. Our

378   model tends more often to underestimate the catchment area, while its yearly mean discharge is overestimated,

379   except at the Beaucaire station along the Rhone River. The bias can be significant and cannot be explained by

380   the model resolution alone.
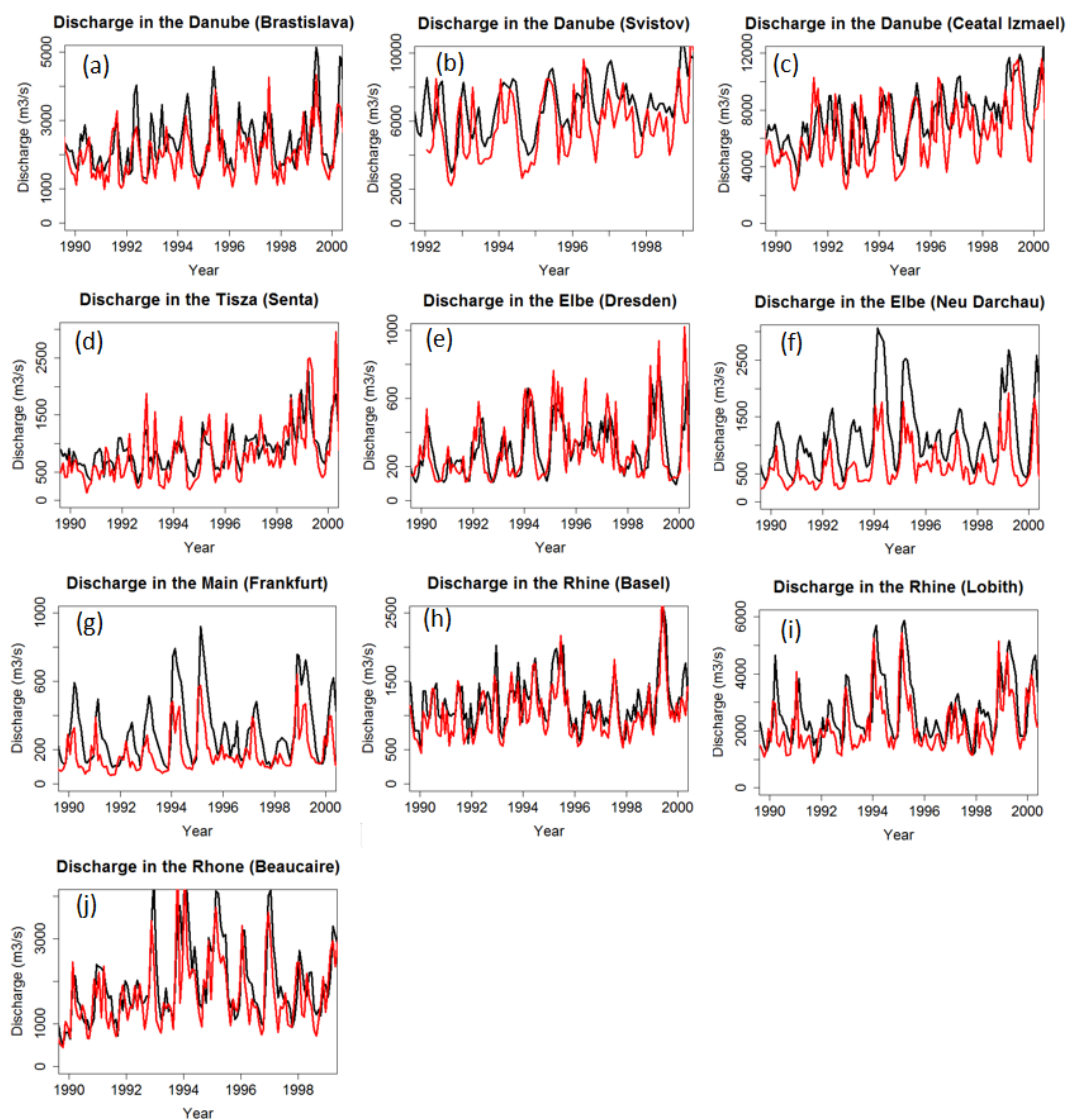
Figure 4. Modeled (black) and observed (red) time series of discharge at the GRDC gauging stations in the Danube (a-c) and its tributaries (d), Elbe (e-f), Rhine and its tributaries (g-i) and Rhone (j). Note the different time periods of measurements. See figure 3 for exact location.

385

To evaluate model performance for discharge, we used the Pearson's coefficient of determination (R^2) and the Nash Sutcliffe modeling efficiency (NSE, Nash and Sutcliffe (1970)). The R^2 only accounts for the correlation with regard to the temporal variability. With R^2 values comprised between 0.43 and 0.62 for all stations, we conclude that the observed seasonality of the discharge along large European rivers is reasonably well reproduced by the model. The NSE not only accounts for the

390 correlation between observed and simulated temporal signals, but also for the model's ability to reproduce absolute discharges. The statistics confirm our previous observation that the model generally overestimates discharges (low NSEs) except for stations Elbe in Dresden, Rhone in Beaucaire, Rhine in Basel and Danube in Bratislava where both the mean and temporality are well captured. Two stations have negative NSE values, which means that the error variance estimated by the model is significantly larger than the variance of the observations; in others words, the difference between model and

395 observations is significant. The mean error (%), that is the weighted difference between the average from the model and the one from observation, confirms that low NSEs are mostly due to overestimated discharges, which is further demonstrated by high mean errors. More results for other European catchments can be found in table S3.

3.1.2 NPP, biomass and soil organic C stocks

400 We briefly compare simulated NPP with the gridded observation-based products GIMMS and CARDAMON (section 2.2.2) as C fixation by the vegetation exerts an important control on DOC stocks in the soil and thus on DOC leaching. We first perform our comparison over a large domain comprised between -10° and 30° in longitude east and 35° and 70° in latitude north - covering the area from Ireland to the Western Black Sea (where the Danube flows into) and from the south of Spain to the north of Scandinavia. Over this area (referred to as "Europe" from here onwards), the modeled yearly averaged NPP

405 amounts to 445 gC m^{-2} yr^{-1}, a value in remarkable agreement with both GIMMS and CARDAMOM estimates of 430 gC m^{-2} yr^{-1} and 460 gC m^{-2} yr^{-1}, respectively. Those two datasets are entailed with an uncertainty that we assume similar to that reported for the MODIS dataset, i.e. 20% (Turner et al 2006). The total living biomass in Europe is simulated at 15.5 PgC or 2.3 kgC m^{-2}. This value is in good agreement with the recent estimate by Avitabile and Camia 2018, which report a biomass stock at around 16 PgC. We estimate that the total soil carbon stock amounts to 58 PgC. Averaged over the first meter of the

410 soil horizon, this corresponds to a value of 9.5 kgC m^{-2} which is comparable to that of HWSD (6 kgC m^{-2}) when using the SOTWIS method to compute the bulk density, but significantly lower when applying Saxton's method (22 kgC m^{-2}), plausibly because the latter overestimates the bulk density in OC-rich soils (Kochy et al., 2015).

Table 2 summarizes the yearly average NPP at the scale of the five selected European catchments. Simulated NPP is of the same order of magnitude as both observation based datasets, without any systematic bias towards an underestimation or

415 overestimation. To provide error bounds for the observational products, we calculated the average standard deviation between yearly-mean values. For GIMMS, we also included the standard deviation induced by the use of the five distinct meteorological forcing files to assess the NPP (section 2.2.1). We find that our simulated catchment averaged NPP fall within the error bounds of the observational products for the Rhine and the Rhone while for the Danube, Elbe and Seine, simulated NPP is slightly above the upper error range.

420 Table 2 reports the biomass and soil carbon (SOC) stocks for the 5 river basins. SOC stocks are usually slightly overestimated compared to HWSD. Results have also been aggregated at the intermediate scale of broad climate zones to analyze how well our model performs for distinct climate regimes. Again the method to calculate the bulk density (section 2.2.2) leads to large uncertainties in observed SOC stocks. Nevertheless, we find that simulated SOC stocks for the warmer climates (Semi-arid and Mediterranean) match well the SOC stocks of the HWSD. However, for other regions, we

425 systematically underestimate the SOC stock compared to HWSD using the Saxton Method, especially in the subarctic climate, but we are closer to the observed values relying on the SOTWIS method for the bulk density. This result is expected since the model does not represent peatlands, which contain important quantities of SOC (Leifeld and Menichetti 2018).

Table 2 Comparison of modeled NPP (1982-2006) against estimates from the CARDAMOM (2001-2010) and GIMMS (1982-2006)
datasets. The mean of the two datasets, along with an assessment of the uncertainty (based on MODIS) and of the standard
deviation are also reported. In addition, the modeled biomass stock and soil organic carbon (SOC) content (first 1m) are compared
with values reported in the HWSD database, using two methods (Saxton and SOTWIS) to calculate the soil bulk density. All
variables and processes are reported for the large-scale basins of focus in this study (see fig. 3 for location), the main climate zones
of continental Europe and the whole model domain.

Basin	NPP gC m⁻² yr⁻¹ ORCHILEAK 1982-2006	NPP gC m⁻² yr⁻¹ Cardamom 2001-2010	NPP gC m⁻² yr⁻¹ GIMMS 1982-2006	Mean gC m⁻² yr⁻¹	Uncertainty 20%	Standard deviation gC m⁻² yr⁻¹	BIOMASS stock kgC m⁻²	SOC kgC m⁻²	HWSD SOC stock (Saxton) kgC m⁻²	HWSD SOC stock (SOTWIS) kgC m⁻²
Danube	560	524	465	495	99	19	3.1	9.3	7.7	5.1
Rhine	527	601	482	542	108	55	1.5	9.5	9.1	5.7
Elbe	576	507	452	480	96	17	2	10.3	17.1	4.9
Rhone	497	593	504	549	110	38	1.4	8.2	5.3	4.5
Seine	667	484	485	484	97	0.5	1.3	9	4.4	3.6
Semi-Arid	264	199	246	222	44	32	0.4	3.3	3.9	4.1
Mediterranean	390	383	386	385	77	21	1.7	5.3	5.1	4.6
Oceanic	561	535	511	523	104	2	1.7	10	23.1	5.6
Humid continental	526	502	458	480	96	11	3.1	10.7	17.2	5.9
Subarctic	338	400	388	394	79	26	2.2	12.2	44.7	7.8
Tundra	344	451	347	399	80	18	2	9.1	5.2	4.3
Europe	445	460	430	441	88	11	2.3	9.5	22	6

3.1.3 Soil DOC stocks

Comparison between observed and modeled DOC stocks and fluxes is more difficult than for biomass and SOC because

440 those have not been assessed at large spatial scales. Nevertheless, representative soil DOC concentration profiles for coniferous and broadleaved forests of Europe have been compiled by Camino et al. (2014). These profiles were used to evaluate our model. Overall, we found that ORCHILEAK slightly overestimates DOC concentrations, especially in the very topsoil horizons with modeled values around 100 mg l^{-1} against 40-60 mg l^{-1} in the observations (Fig. 5). We also simulated higher concentrations in broadleaved forests than in coniferous forests while Camino et al. (2014) obtained the opposite.

445 When integrated over the first meter of the soil horizon of forested ecosystems (28 % of the surface area), the modeled and observed DOC stocks amount to 22.2 and 11.3 gC m^{-2}, respectively. The underestimation of SOC stocks combined with a likely overestimation of DOC stocks suggests that SOC decomposition rates in the new soil carbon module may be slightly too high. It is however difficult to generalize this conclusion because of the lack of synthesis data for other land cover types, especially croplands and grasslands which together represent about 50 % of the total European land area. Modeled DOC

450 stocks averaged over broad climate regions reveal highest values for the oceanic climate with 32 gC m^{-2} and the Mediterranean climate with 26 gC m^{-2}. Semi-arid and humid continental climates have similar concentrations of respectively 17.5 and 20 gC m^{-2} and it is in the coldest climates (subarctic and tundra) that we find the lowest DOC concentrations around 8 gC m^{-2}.
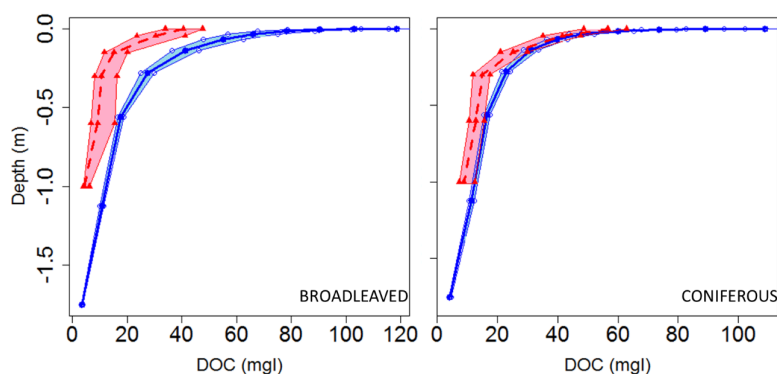
455 **Figure 5. Modelled (blue) versus observed (red dashed) DOC concentration profiles averaged over the soils of the European Coniferous and Broadleaved forest biome. Data from Camino et al. (2014). The shaded area represents the 95% bootstrap confidence interval for model and observations.**

3.1.4 DOC leaching fluxes

460 The model simulates a yearly-mean DOC leaching flux over Europe of 14.3 (±10) TgC yr^{-1} (Fig 6), the standard deviation being here coarsely approximated by spatial variability. The average area specific flux rates is of 2.6 (±2.5) gC m^{-2} yr^{-1}. We compared DOC leaching fluxes with site level observations from Kindler et al. 2011, across 17 local measurements, each sampled fortnightly during the period October 2006 until March 2008. Our modeled average of 2.6 (±2.5) gC m^{-2} yr^{-1} is of the same order of magnitude as the observed one (4.2 gC m^{-2} yr^{-1}). Although the modeled mean is about 38 % lower than the

465 one measured, the standard deviation representing the spatial variability in simulated DOC leaching fluxes over all our model grid cells encapsulate the observational mean, highlighting a significant heterogeneity that is difficult to embrace with local measurements alone.
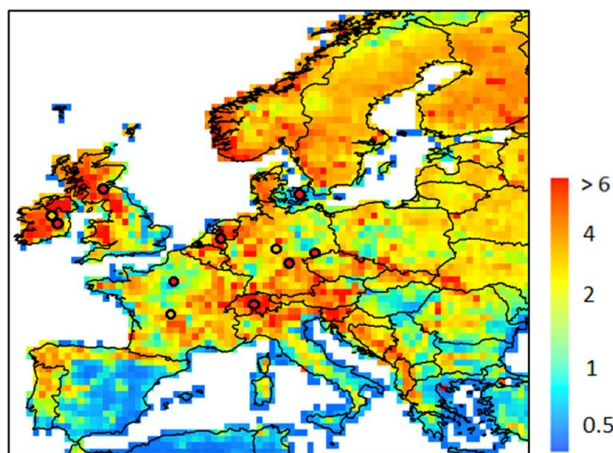
Figure 6. Modelled yearly mean terrestrial DOC leaching flux (period 1979-2006) to the river European river network (in gC m^{-2}
470 **yr^{-1}). The local observations from Kindler et al., 2010 are also reported, using the same scale. Note that the local observations**
cover a much shorter time period and may not be representative of the whole year.

The seasonal distribution of the DOC leaching flux is shown in Fig. 7. On average, the leaching flux per season averaged
over Europe amounts to 1.6, 1.3, 0.5 and 1.4 TgC month^{-1} in winter, spring, summer and autumn, respectively. If we exclude
475 the high latitude and high altitude regions (Scandinavia, the Alps), a clear seasonality is observed with the lowest fluxes in
summer and spring and highest fluxes in winter and autumn. In the high latitude/altitude regions, the pattern is different with
highest fluxes in spring which extends to the summer in the Alps, and corresponds to the snowmelt period. The highest
fluxes per unit area are simulated in Scandinavia during the spring season, even though peatlands are not represented in the
model. Some regions are leaching hotspots such as the Alps throughout the year, the West Balkans during autumn and the
480 Western flank of the UK in autumn and winter. This is mainly due to the high local runoffs and thus runoff rates in these
regions.
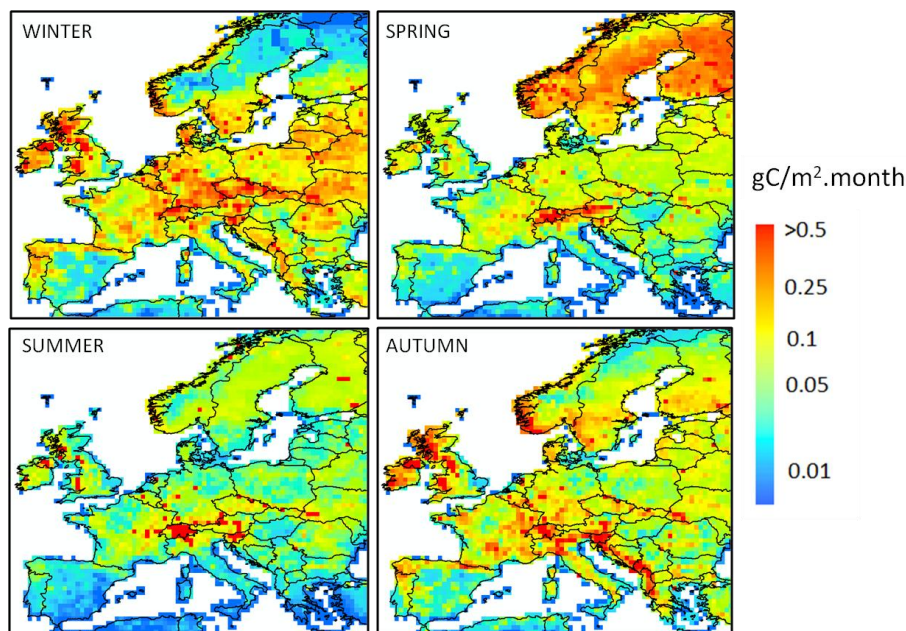
Figure 7. Seasonal distribution of the terrestrial DOC leaching flux (gC m⁻² month⁻¹), average over the period 1979-2006. A logarithmic scale is used to better highlight the spatiotemporal gradients.

485

3.1.5 Fluvial DOC decomposition and export fluxes

The export of DOC from the European river network to the coast is arguably the best monitored variable against which our model can be evaluated. Using this flux to build confidence in our estimate of the terrestrial DOC leaching requires an assessment of the DOC degradation within rivers, a process that is controlled by the hydrology and the half-lives of reactive

490 DOC compounds. In the model, the first-order decomposition rates at a given temperature of 28°C are equal to 0.3 d⁻¹ and 0.01 d⁻¹ for the labile and refractory DOC pools, respectively. Based on those values and the simulated distribution of labile and refractory DOC, the estimated bulk decomposition rate constant averaged over the entire model domain is equal to 0.05 d⁻¹, which corresponds to a half-life for DOC of about 14 days (Table 3). This rate constant varies across Europe but always remains within the same order of magnitude, with half-lifes ranging from 6 to 20 days (0.035-0.122 d⁻¹). These

495 decomposition rates are in good agreement with the average rate reported by Berggren and Al-Kharusi. (2020) of 0.037 d⁻¹ based on field experiments carried out at multiple river sampling locations across Europe. We thus conclude that DOC decomposition rates used in ORCHILEAK are reasonable, and fluvial DOC fluxes are a valid proxy to evaluate simulated DOC leaching fluxes.

500 **Table 3. Estimated river DOC decay rates applied in ORCHILEAK. Values are reported for four large river catchments and for the six dominant climate zones**

REGIONS		DECAY RATES (day^{-1})
BASIN	Rhine	0.074
	Danube	0.043
	Meuse	0.056
	Rhône	0.072
CLIMATE ZONE	Semi-arid	0.035
	Mediterranean	0.046
	Oceanic	0.053
	Humid continental	0.048
	Subarctic	0.064
	Tundra	0.122
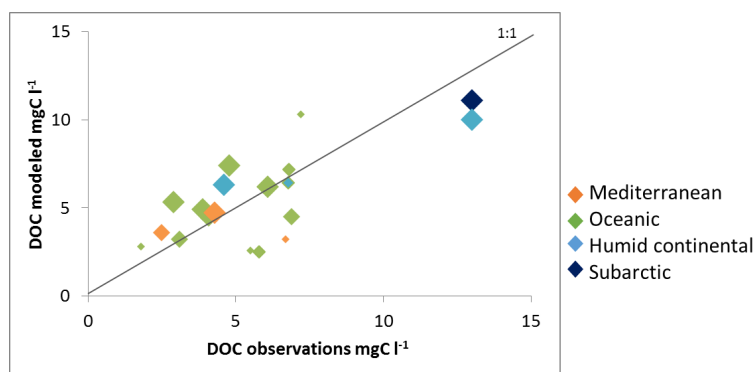
Figure 8. Modelled river DOC concentration against observed values. The color code indicates the dominant climate zone for each
505 **catchment while the size of the diamond is proportional to the catchment area according to the following classes: < 10 000 km², < 50 000 km², < 100 000km² and > 100 000 km². See table S4 for further details.**

Figure 8 compares modeled versus observed multi-annual mean DOC concentration at specific locations or within a group of small river catchments. Local DOC measurements include data near the mouth of the Rhine, Elbe, Rhône and Seine rivers
510 (discharge, DOC concentration and fluxes for the Rhine and Seine in figure 9). In addition, Abril et al. (2002) report DOC concentrations measured at nine river mouths discharging along the Atlantic façade and the North Sea, three of which (Rhine (NL), Scheldt (BE) and Gironde (F)) resolve the seasonality while the other six (Elbe (GE), Ems (GE), Thames (UK), Loire (FR), Sado (P), Douro (P)) only rely on a single measurement per year. Both GLORICH and Abril et al. (2002) report DOC concentrations at the mouth of the Rhine and the Elbe but their values diverge because in addition to analytical uncertainties,
515 the sampling period and data density are not the same. Measured values are equal to 4.3 and 2.9 mg C l^{-1} for the Rhine and 4.6 and 6.1 mg C l^{-1} for the Elbe, respectively highlighting inherent variability in observational data. To complement these local samplings, we also compared our simulated DOC concentrations with those of Mattson et al. (2008) for several groups of catchments in Finland (9 spread over the whole country), Denmark (10 draining into Horsens fjord), the UK (10 draining into the River Conwy) and France (5 draining into the River Tech). All measured DOC concentrations ranged from 2.5 mg C

520   l^{-1} to 10 mg C l^{-1} except in two regions in the north (Finland and basins flowing into the Baltic sea) where concentrations exceeded 10 mg C l^{-1}. For most of the data, the model slightly overestimated the river DOC concentrations. The model results also suggest that the concentrations broadly increase with latitude, with the higher values found in humid continental and subarctic climate and the lower ones in the Mediterranean climate, a result in agreement with the observations from Mattson et al. (2008). Such pattern possibly results from decreasing mean annual air temperature and runoff in Northern

525   Europe that favor incomplete decomposition of litter and DOC, thus favouring DOC production, while at the same time DOC turnover rates in the soils are decreased. Also the increased abundance of forests, and in particular coniferous forests, is a valid explanation for higher DOC leaching (Lauerwald et al. 2012). However, it is important to keep in mind that we're missing the peatlands, suggesting that we could lack part of the DOC leaching in subarctic and tundra regions leading to even higher DOC fluxes further in the North. Finally, the comparison reveals that model performance tends to improve with

530   catchment size, likely reflecting the difficulty to capture the DOC dynamics at the small scale with the current resolution of ORCHILEAK. But overall, our model is capable of reproducing observed yearly mean DOC concentrations for a wide range of river basins spread between Finland and Portugal.
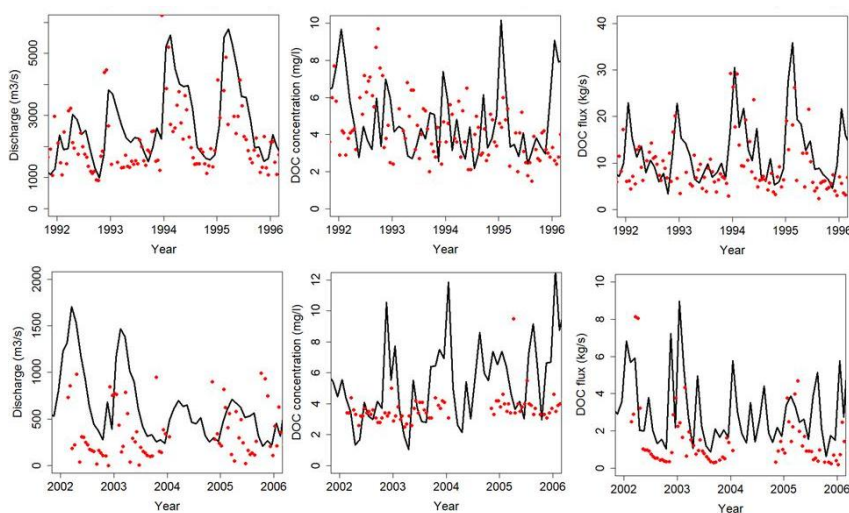
535   **Figure 9. Time series of discharge (left), DOC concentration (middle) and DOC fluxes (right) in the river Rhine at Lobith (top row, period 1992-96) and in the Seine at Poses (bottom row, period 2002-2006. See figure 3 for location of stations.**

The temporal evolution of observed river DOC fluxes is only available at four stations (Rhine, Elbe, Rhône and Seine) where DOC time series have been recorded over multi-annual periods (Fig. 9). The multi-year mean modeled DOC fluxes are

540   estimated for the Rhine, Elbe, Rhone and Seine at 11.9, 7.2, 8.8 and 3.2 kg s^{-1}, respectively. The observations amount respectively to 7.9, 3.6, 4.6, 1.6 kg s^{-1}. For all stations, the model thus overestimates slightly fluvial DOC fluxes, which is not surprising since the model tends to overestimate the discharge. At these four stations, ORCHILEAK also slightly overestimates river DOC concentrations except for the Seine where concentrations are largely underestimated and discharge largely overestimated. In terms of temporal correlation, the simulated DOC flux for the Rhone compared to the observed one

545   yields a R^2 of 0.6 and a mean error of 92% (results for the Seine, Elbe and Rhine are reported in supplementary table S5). In figure 8, we clearly see a large overestimation of the temporal variability in DOC concentrations and this could lead to an overestimation in DOC fluxes since there is a positive relationship between concentrations and discharge. The overestimation of DOC concentrations and consequently of DOC fluxes could be due to high DOC leaching.

The overestimation of DOC fluxes can also be due to the fact we choose to not recalibrate the hydrology scheme but instead
550 we optimized the model for the discharge by adjusting the surface roughness of the vegetation (section 2.2.1). Since those
four stations are all located in the same region with the same type of land cover (Western Europe), two other locations have
been selected: England and the Baltic Sea. For those two locations, there are no time series data for DOC flux but some
studies have measured DOC concentrations/fluxes. Worrall et al. (2012) estimated DOC concentration across UK and
Fransner et al. (2016) reported modelled DOC concentrations for all the catchments flowing into the Baltic Sea.

555 Finally, although the model-data comparison points to a slight overestimation of the river DOC export flux, our pan-
European estimate amounts to 12.3 TgC yr^{-1}. This estimate is in fact about 35 % lower than the one reported in another
model study by Li et al. (2019), based on the TRIPLE-HYDRA, a process-based model for which the DOC export flux
reaches 19.3 TgC yr^{-1}. Li et al. (2019) applied the model at the global scale and simulation results were primarily evaluated
against observations in the world-largest rivers and for Europe only included the Volga River. Li et al. (2019) then applied
560 the model for multiple rivers in Europe such as the Danube, the Po, and the Elbe. Despite these different scales of analysis,
the export fluxes predicted by both models fall within the same order of magnitude.

3.1.6 Manure implementation

The implementation of manure significantly affects DOC leaching from grasslands and croplands (Fig. 10) which cover
565 more than half of the studied region. The average annual input rate of manure into the soil is around 2.5 gC m^{-2} yr^{-1} (Fig. 2c).
With manure implementation, the DOC leaching rate increase drastically (average of +72% compared to the DOC leaching
without manure), in particular in the oceanic and humid continental climate regions, where the average DOC leaching rate
changes from 1.6 to 2.7 gC m^{-2} yr^{-1} and 1.7 to 2.5 gC m^{-2} yr^{-1}, respectively. In whole Europe, manure implementation leads
to an increase of total DOC leaching into the river network from 9.8 to 14.3 TgC yr^{-1}.
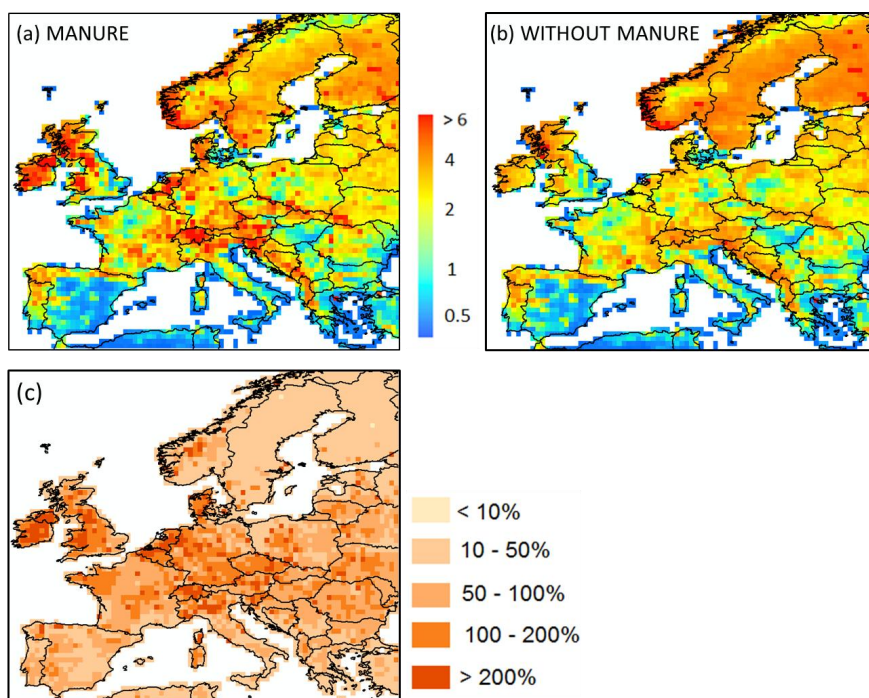
570

**Figure 10. Comparison of modeled yearly mean terrestrial DOC leaching flux (period 1979-2006) to the river European
river network (in gC m^{-2} yr^{-1}), with (a) and without the manure (b). (c) Increase of DOC leaching in percentage compared
to DOC leaching without the manure implementation.**

3.2 European-scale DOC leaching dynamics

575   ### 3.2.1 Drivers of DOC leaching

Here, we analyze what controls the spatial distribution and temporal variability in the DOC leaching. Figure 11 shows seasonal variability of DOC leaching and total runoff (surface runoff plus drainage) in different climate zones of Europe, revealing a clear and consistent relationship between those two fluxes. The seasonal peak in DOC leaching consistently occurs in winter while minimum values are found during summer. These results suggest that both spatial and temporal

580   variability in leaching are correlated to total runoff.
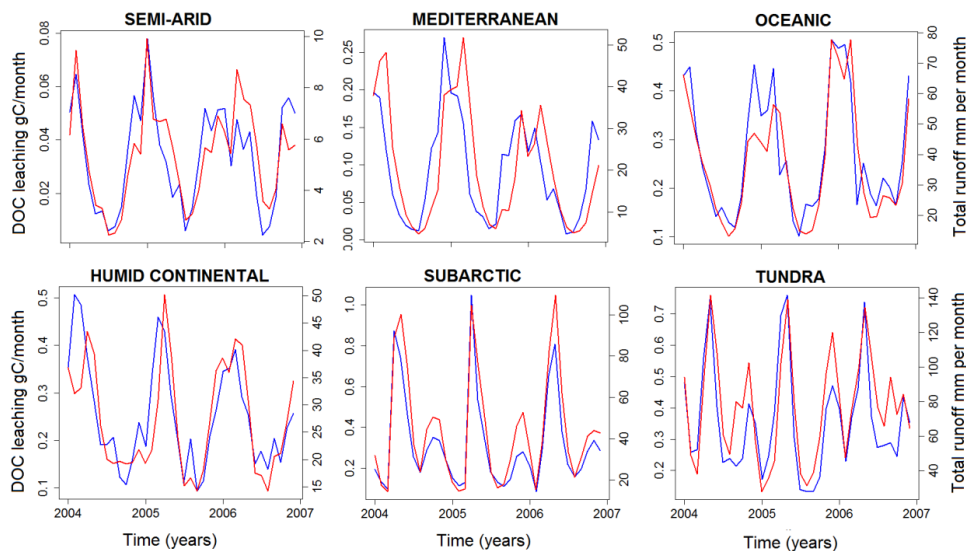
Figure 11. Simulated DOC leaching flux (gC m^{-2} month^{-1}) (blue) and total Runoff (mm per month) (red) for the six largest climate zones (period 2004-2007).

585   To further explore the environmental controls the DOC leaching, we expressed DOC leaching as fraction of terrestrial NPP (Figure 12). Doing this, we assume that NPP, which is undoubtedly the first source for DOC production, is as well an important control of the DOC leaching flux. Moreover, normalizing DOC leaching by NPP, we strive to show the possible influence of other controls, allowing for a more in-depth analysis of the effect of hydrology and climate on the DOC leaching flux. Figure 12 reveals that the fraction of terrestrial NPP lost to DOC leaching increases, as expected, with total

590   runoff. Moreover, this fraction increases with the contribution of surface runoff to total water loss from surface runoff plus drainage (Fig. 12b). This can be explained by the general decrease in soil DOC concentrations with depth (Fig. 5), leading to higher DOC concentrations in surface runoff than in drainage. In fact, according to our simulations, 97% of the leached DOC is concentrated in the surface runoff. Note that higher total runoff is often associated with a higher contribution of surface runoff, which leads to a 'flushing effect' where high runoff events contribute a disproportionate high fraction of the long-

595   term DOC leaching (Idir et al. 1999, Raymond and Saiers 2010). Finally, we found higher leaching to NPP ratios at lower temperatures (Fig. 12a), hinting at the fact that lower temperatures lead to longer turnover times of DOC in the soil, and thus higher concentrations in the leaching flux (section 2.1.2).
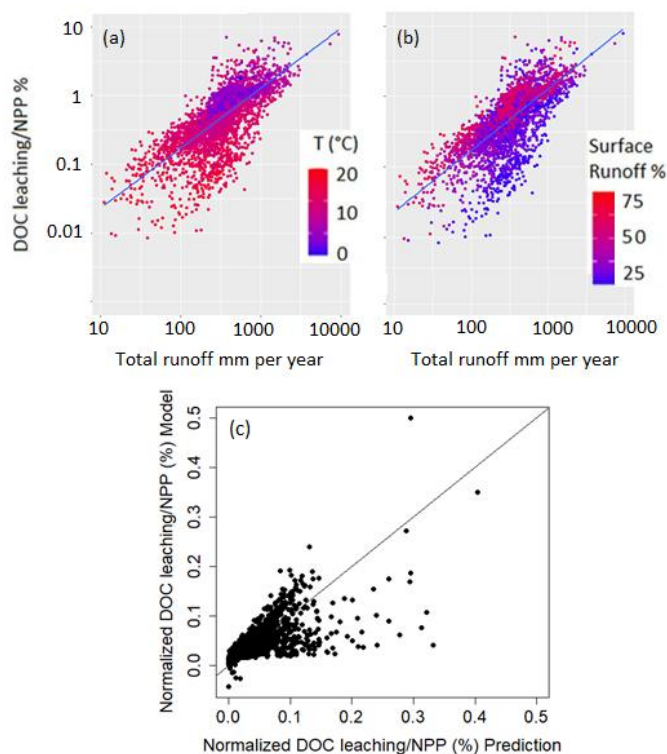
600 **Figure 12. Fraction (%) of terrestrial NPP that is leached as DOC in the river network as a function of total runoff. Each point represents the grid-cell average of both metrics for the entire simulation period (1979-2006). In panel (a) the color scale represents the grid-cell average temperature (°C) while in panel (b), the color scale represents the ratio of surface runoff to total runoff in percentage. Panel (c) the normalized predicted DOC leaching flux to NPP ratio (equation 13) against the normalized simulated values.**

605

To better quantify the effects of all these drivers on DOC leaching, we fitted a multi-linear regression model to predict the ratio of DOC leaching to NPP as a function of surface runoff, drainage and temperature at all grid points and for each month over the simulation period (eq. 13). To compare the importance of each predictor for the spatiotemporal patterns of DOC leaching, we normalized all variables Vs of equation 13 according to equation 14 (where i is the cell index).

$$\frac{DOC\ leaching}{NPP} = K_0 + K_R * Runoff + K_D * Drainage + K_T * e^{T(°C)} \qquad (13)$$

$$K_0 = 0.01 \pm 7 * 10^{-4}$$
$$K_R = 0.342 \pm 0.009$$
$$K_D = 0.276 \pm 0.014$$
$$K_T = -0.055 \pm 0.013$$

610 (p-value $< 2*10^{-16}$ except for temperature where p-value $= 2.7*10^{-5}$)

$$V_{i,N} = \frac{V_i - V_{min}}{V_{max} - V_{min}} \qquad (14)$$

To rule out any significant multi-collinearity in the regression model, we calculated for each predictor the Variance Inflation Factor (VIF). The VIF evaluates the correlations among all predictors which could impact the robustness of the regression model (James et al., 2017). The closer the VIF is to 1, the more robust is the model. In our regression, VIF's of the runoff,

drainage and temperature are respectively 1.13, 1.13 and 1.01, confirming that our prediction is robust and not biased by
615   high multicollinearity.

In Fig. 12 (c), the DOC leaching simulated by ORCHILEAK is compared with the one predicted by equation 13. Our simple
regression model is able to reproduce the simulations with a residual standard error of 0.68% and a R^2 of 0.45. The
coefficients of our regression model reveal that spatio-temporal variability in DOC leaching is mainly driven by the surface
runoff (K_R) and drainage (K_D). Air temperature as third control of DOC leaching is of subordinate importance as reflected by
620   its low predictor's coefficient (K_T).

Table 4 summarizes for each climate zone in Europe the DOC leaching fluxes, in total numbers and normalized by NPP, as
well as other important components of the terrestrial C budget. Since runoff and temperature were identified as the
controlling factors of the DOC leaching flux, normalized DOC leaching fluxes are expected to be significantly different
among climate zones. Indeed, the fraction of NPP lost to the river network as DOC is the lowest in the semi-arid region
625   (0.13%) where annual precipitation is low (total runoff around 92 mm per year) and temperatures are high.

Table 4. Key physical and biogeochemical characteristics of the six dominant climate zones of the European domain.

Variables	Unit	Semi-arid	Mediterranean	Oceanic	Humid continental	Subarctic	Tundra
Area	km²	3.01E+11	8.74E+11	1.38E+12	2.11E+12	9.03E+11	1.56E+11
Leaching		0.35	1.01	2.73	2.5	2.84	4.2
NPP	gC m⁻² yr⁻¹	264.1	389.9	561.3	526.4	338.3	344.2
HR		175.5	278.6	390.6	345.7	255.3	266.9
Harvest (crop)		74.7	68	111.8	112.6	15.7	30.5
Harvest (wood)		5.4	25	46.1	40.7	41	41.8
LUC		-0.04	-4.8	-5.3	-7.7	-15.9	-3.7
NEE calculated		87	107.5	160	175	82.1	73.7
Leaching/NPP	%	0.13	0.26	0.49	0.48	0.84	1.22
Leaching/NEE		0.4	0.94	1.71	1.43	3.46	5.7
Runoff	Mm yr⁻¹	30	63	82	91	236	404
Drainage		62	229	406	236	290	517
Temperature	°C	15	14.6	10.4	7.8	1.8	4.6

630   The highest fraction of NPP exported to rivers as DOC is found in the tundra climate and reach 1.22%. That can be explained by high runoff and drainage (reaching 920 mm per year) in this climate zone, but also by low temperatures lowering the fraction of DOC already decomposed within the soil column. The subarctic climate also presents a similarly high DOC leaching to NPP ratio with a value of 0.84%. The Mediterranean, Oceanic and humid continental climate zones present intermediate DOC leaching to NPP ratios of respectively 0.26%, 0.48% and 0.49%. Averaged over the whole of the

635   EU-27, the DOC leaching flux normalized to the NPP amounts to 0.60 %.

3.2.2 Comparison with previous assessments of DOC leaching

In one of the first studies on the terrestrial C budget of Europe (Janssens et al., 2003) an imbalance (missing sink) between atmospheric CO_2 inversions and bottom up C stock change accounting was partly attributed to the loss of carbon from land

640   to rivers in the form of DOC of around 4 gC m^{-2} yr^{-1}. Our results, 2.6 ± 2.5 gC m^{-2} yr^{-1}, support this hypothesis although we suggest a DOC leaching rate slightly lower than this early study. Our lower value may come from the fact that we did not simulate peatlands and organic soils which are known hotspots of DOC leaching (Leifeld and Menichetti 2018), in particular in areas such as the northern UK and Scandinavia. In terms of temporal variability, we found the highest DOC leaching in winter averaged over the continent (8.9 TgC in total for the six months of winter October to March) and the lowest in

645   summer (5.4 TgC over the period April to September), consistent with the findings of Kindler et al. (2011). In terms of drivers of the DOC leaching fluxes, our results are in line with empirical findings by Gielen et al. (2011) that identified hydrology as the main driver of the inter- and intra-annual variability in DOC leaching. Similar conclusions have also been drawn by other empirical studies (Michalzik et al., 2001, Neff and Asner 2001, Worrall and Burt 2007).

It is also interesting to compare our results with recent global and regional model studies of DOC leaching in tropical and

650   boreal ecosystems. For the Amazon and Congo basins, Hastie et al. (2019, 2021) found that 12 and 4 % of the NPP is exported each year to inland waters in the form of DOC, respectively – much higher than the one we report for Europe as a whole (0.6%). Note that for these tropical lowland river basins extensive riparian wetlands are an important source of DOC, which are of lower importance in Europe. For the Lena river basin located in the boreal region, Bowring et al. (2020) found a DOC leaching of NPP ratio of about 1.5%. In our model assessment, this ratio reaches a very similar value of 1.2% for the

655   boreal portion of Europe. For the temperate zone, a ratio of 0.35% for the East Coast of the US can be calculated when dividing the average DOC leaching flux of 2.7 gC m^{-2} yr^{-1} simulated by Tian et al., 2015 by the average NPP of 780 gC m^{-2} yr^{-1} estimated by Zhao et al., (2005). Further, our value is quite similar to the one extracted from the global study by Nakhavali et al. (2020) that amounts to 0.5 % for the European domain only. Overall, this comparison highlights that in Europe, the fraction of NPP lost as DOC to the river network is significantly smaller than in other regions of the world. The

660   lower value is likely due to the lower connectivity between terrestrial and aquatic systems due to the lack of extensive wetlands, which have been reduced by major regulation of the European river network.

3.2. 3 Implications for the terrestrial carbon budget of Europe

The terrestrial carbon budget is controlled by NPP, heterotrophic respiration, crop and wood harvesting and land use change.

665   Here we look at the net ecosystem exchange (NEE) which is the net C exchange between land and atmosphere (Kramer et al., 2002). However, this view neglects the leakiness of terrestrial ecosystems that permanently removes a fraction of the land C and export it to the river network. Moreover, we can argue that DOC leaching represents a fraction of NEE, while the remainder of NEE can be attributed to harvest, land use change and changes in biomass and soil C stocks. From 1979 to 2012, the average NEE in Europe is 860 TgC yr^{-1} (123 gC m^{-2} yr^{-1}), equaling about 28% of the total NPP (Fig. 13b). The

670   ratio of DOC leaching to NEE shows drastic spatial variation, varying from an average value of 0.4% in the semi-arid regions to a value of 5.7% in the tundra. In whole Europe, the DOC leaching is about 3% of the NEE.
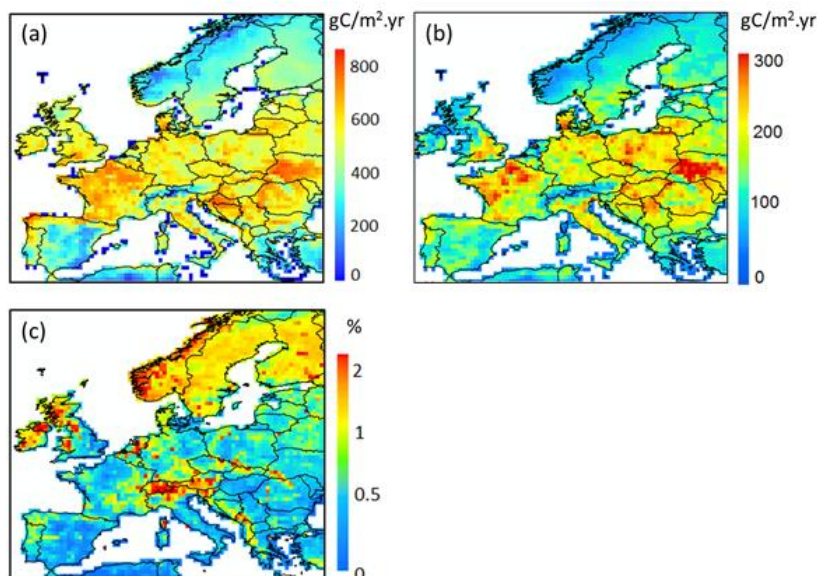
Figure 13. Grid-cell average (a) Net Primary Production, (b) Net Ecosystem Exchange and (c) fraction of NPP leached to the river network as DOC (%) for the period 1979-2006

675 **4 Conclusion**

We reconstructed the terrestrial and riverine C fluxes in Europe during period 1979-2012 using the ORCHILEAK LSM. The total C leaching from soil to European rivers is 14.3 TgC yr^{-1} on average, about 0.6 % of the estimated NPP and 3% of the terrestrial net up-take of atmospheric C. This flux shows large spatial and temporal variations. In specific, DOC leaching overall increases from warm and dry regions to cold and wet regions. However, since the model does not represent peatlands

680 yet, the simulation results for subarctic and tundra regions in northern Europe could be biased. In whole Europe, DOC leaching rate is the highest in winter and lowest during the summer, mainly controlled by the seasonal variation of runoff. The implementation of manure lead to a significant increase in DOC leaching over the oceanic and humid continental region where croplands and grasslands are dominant. Our results contribute to a better assessment of the land-ocean C fluxes in Europe and to a better understanding of the effects of lateral C transfer on the terrestrial C budget. Combined with recent

685 large-scale studies in tropical and boreal biomes as well as along the east coast of the US, an emergent view regarding the global role of DOC leaching on the terrestrial C balance and its underlying drivers is progressively emerging.

Code and data availability

The model code used in this study is available at DOI : 10.14768/75AC2F47-4691-46AF-9B12-B1A9629CBC56

690 All forcing data set are listed in table 1. Data of observed discharge used in this study are available from the Global Runoff Data Center (GRDC) at www.bafg.de/GRDC. Data of observed DOC concentrations in France are provided by eau de France at http://www.data.eaufrance.fr/.

Supplement

695 The supplement related to this article is available in the attached file (pdf).

Author contribution

700 CG, RL, PR, PC designed the study. CG performed calibration and evaluation of the model, ran the simulations, and wrote the initial manuscript. RL updated the model code of ORCHILEAK to improve representation of soil hydrology and DOC cycling. HZ implemented the representation of manure impacts on soil DOC dynamics into the model code. All co-authors contributed to interpretation of model results and improvement of the manuscript.

705 **Competing interests**

The authors declare that they have no conflict of interest.

Acknowledgements

RL, PC and BG acknowledge funding from the French state aid managed by the ANR under the "Investissements d'avenir"
710 programme [ANR-16-CONV-0003]. HZ, PR and RL acknowledge the 'Lateral-CNP' project (No. 34823748) supported by the Fonds de la Recherche Scientifique –FNRS. CG and PR acknowledges funding from the European Union's Horizon 2020 research and innovation programme under Grant Agreement 776810 (project VERIFY).

References

Abril G., M. Nogueira, H. Etcheber, G. Cabeçadas, E. Lemaire, M. Brogueira. Behaviour of organic carbon in nine
715 contrasting European estuaries Estuar. Coast. Shelf Sci., 54 (2002), pp. 241-262

Avitabile, V., Camia, A., 2018. An assessment of forest biomass maps in Europe using harmonized national statistics and inventory plots. For. Ecol. Manage. 409, 489–498.

720 Berggren, M. Al-Kharusi, E.S. Decreasing organic carbon bioreactivity in European rivers. Freshw. Biol., 65 (6) (2020), pp. 1128-1138, 10.1111/fwb.v65.610.1111/fwb.13498.

Bloom, Anthony; Williams, Mathew. (2015). CARDAMOM 2001-2010 global carbon Model-Data Fusion (MDF) analysis, 2001-2010 [dataset]. University of Edinburgh. School of GeoSciences. https://doi.org/10.7488/ds/316.
725

Bowring, S. P. K., Lauerwald, R., Guenet, B., Zhu, D., Guimberteau, M., Tootchi, A., Ducharne, A., and Ciais, P (2019): ORCHIDEE MICT-LEAK (r5459), a global model for the production, transport, and transformation of dissolved organic carbon from Arctic permafrost regions – Part 1: Rationale, model description, and simulation protocol, Geosci. Model Dev., 12, 3503–3521, https://doi.org/10.5194/gmd-12-3503-2019, 2019.
730

Bowring, S. P. K., Lauerwald, R., Guenet, B., Zhu, D., Guimberteau, M., Regnier, P., Tootchi, A., Ducharne, A., and Ciais, P.: ORCHIDEE MICT-LEAK (r5459), a global model for the production, transport, and transformation of dissolved organic carbon from Arctic permafrost regions – Part 2: Model evaluation over the Lena River basin, Geosci. Model Dev., 13, 507–520, https://doi.org/10.5194/gmd-13-507-2020, 2020.

735 Camino-Serrano, M., Gielen, B., Luyssaert, S., Ciais, P., Vicca, S., Guenet, B., Vos, B. De, Cools, N., Ahrens, B., Altaf Arain, M., Borken, W., Clarke, N., Clarkson, B., Cummins, T., Don, A., Pannatier, E. G., Laudon, H., Moore, T., Niemi­nen, T. M., Nilsson, M. B., Peichl, M., Schwendenmann, L., Siemens, J., and Janssens, I.: Linking variability in soil so­lution dissolved organic carbon to climate, soil type, and vegetation type, Global Biogeochem. Cy., 28, GB004726, https://doi.org/10.1002/2013gb004726, 2014.

740

Camino-Serrano, M., Guenet, B., Luyssaert, S., Ciais, P., Bastrikov, V., De Vos, B., Gielen, B., Gleixner, G., Jornet-Puig, A., Kaiser, K., Kothawala, D., Lauerwald, R., Peñuelas, J., Schrumpf, M., Vicca, S., Vuichard, N., Walmsley, D., and Janssens, I. A.: ORCHIDEE-SOM: modeling soil organic carbon (SOC) and dissolved organic carbon (DOC) dynamics along vertical soil profiles in Europe, Geosci. Model Dev., 11, 937–957, https://doi.org/10.5194/gmd-11-937-2018, 2018.

745

Campoy, A., Ducharne, A., Cheruy, F., Hourdin, F., Polcher, J., and Dupont, J. C.: Response of land surface fluxes and precipitation to different soil bottom hydrological conditions in a general circulation model, J. Geophys. Res.-Atmos., 118, 10725–10739, https://doi.org/10.1002/Jgrd.50627, 2013.

750   Ciais, P., et al. (2013), Carbon and other biogeochemical cycles, in Climate Change 2013: The Physical Science Basis. Contribution of Working Group I to the Fifth Assessment Report of the Intergovernmental Panel on Climate Change, edited by T. F. Stocker et al., Cambridge Univ. Press, Cambridge, U. K., and New York.

Cole, J.J., Prairie, Y.T., Caraco, N.F., McDowell, W.H., Tranvik, L.J., Striegl, R.G., Duarte, C.M., Kortelainen, P.,
755   Downing, J.A., Middelburg, J.J., Melack, J., 2007. Plumbing the global carbon cycle: integrating inland waters into the terrestrial carbon budget. Ecosystems 10 (1), 171–184.

Drake, T. W., P. A. Raymond, and R. G. M. Spencer. 2018. Terrestrial carbon inputs to inland waters: a current synthesis of estimates and uncertainty. Limnology and Oceanography Letters 3:132–142. http://doi.org/10.1002/lol2.10055

760

FAO/IIASA/ISRIC/ISS-CAS/JRC, 2012. Harmonized World Soil Database (version 1.2). FAO, Rome, Italy and IIASA, Laxenburg, Austria.

Fransner F, Nycander J, Mörth C-M et al (2016) Tracing terrestrial DOC in the Baltic Sea—a 3-D model study. Global
765   Biogeochem Cycle 30:134–148. doi:10.1002/2014GB005078

Friedlingstein P., O'Sullivan M., Jones M.W., Andrew R.M., Hauck J., Olsen A., *et al.* **Global carbon budget 2020**. Earth Syst Sci Data, 12 (2020), pp. 3269-3340, 10.5194/essd-12-3269-2020

770   Gielen, B., Neirynck, J., Luyssaert, S., and Janssens, I. A.: The importance of dissolved organic carbon fluxes for the carbon balance of a temperate Scots pine forest, Agr. Forest Meteorol.,151, 270–278, https://doi.org/10.1016/j.agrformet.2010.10.012,2011.

Goll, D. S., Vuichard, N., Maignan, F., Jornet-Puig, A., Sardans, J., Violette, A., Peng, S., Sun, Y., Kvakic, M.,
775   Guimberteau, M., Guenet, B., Zaehle, S., Penuelas, J., Janssens, I., and Ciais, P.: A representation of the phosphorus cycle for ORCHIDEE (revision 4520), Geosci. Model Dev., 10, 3745-3770, https://doi.org/10.5194/gmd-10-3745-2017, 2017.

Guimberteau, M., Drapeau, G., Ronchail, J., Sultan, B., Polcher, J., Martinez, J.-M., Prigent, C., Guyot, J.-L., Cochonneau, G., Es- pinoza, J. C., Filizola, N., Fraizy, P., Lavado, W., De Oliveira, E., Pombosa, R., Noriega, L., and Vauchel, P.:
780   Discharge sim- ulation in the sub-basins of the Amazon using ORCHIDEE forced by new datasets, Hydrol. Earth Syst. Sci., 16, 911–935, https://doi.org/10.5194/hess-16-911-2012, 2012.

Guimberteau, M., Zhu, D., Maignan, F., Huang,Y.,Yue, C., Dantec- Nédélec, S., Ottlé, C., Jornet-Puig, A., Bastos, A., Laurent, P., Goll, D., Bowring, S., Chang, J., Guenet, B., Tifafi, M., Peng, S., Krinner, G., Ducharne, A., Wang, F., Wang, T., Wang, X., Wang, Y., Yin, Z., Lauerwald, R., Joetzjer, E., Qiu, C., Kim, H., and Ciais, P.: ORCHIDEE-MICT (v8.4.1), a land surface model for the high latitudes: model description and validation, Geosci. Model Dev., 11, 121–163, https://doi.org/10.5194/gmd-11-121- 2018, 2018.

Hartmann, J., Lauerwald, R., and Moosdorf, N.: A brief overview of the GLObal RIver CHemistry Database, GLORICH, Procedia, Earth Planet. Sci., 10, 23–27, 2014.

Hastie, A., Lauerwald, R., Ciais, P., Regnier, P (2019). Aquatic carbon fluxes dampen the overall variation of net ecosystem productivity in the Amazon basin: An analysis of the interannual variability in the boundless carbon cycle. Global Change Biology,; 25: 2094– 2111. https://doi.org/10.1111/gcb.14620

Hastie, A., Lauerwald, R., Ciais, P., Papa, F., and Regnier, P.: Historical and future contributions of inland waters to the Congo basin carbon balance, Earth Syst. Dynam. Discuss., https://doi.org/10.5194/esd-2020-3, , 2021.

Idir, S., A.Probst, D.Viville, and J. L.Probst (1999), Contribution of saturated areas and hillslopes to the water and element fluxes exported during a storm event: Tracing with dissolved organic carbon and silica. The Strengbach catchment case study (Vosges, France), *C. R. Acad. Sci., Ser. II*, **328**(2), 89– 96, doi:10.1016/s1251-8050(99)80003-2.

James, Gareth; Witten, Daniela; Hastie, Trevor; Tibshirani, Robert (2017). An Introduction to Statistical Learning (8th ed.). Springer Science+Business Media New York. ISBN 978-1-4614-7138-7

Janssens, I. A., Freibauer, A., Ciais, P., Smith, P., Nabuurs, G. J., Folberth, G., Schlamadinger, B., Hutjes, R. W. A., Ceulemans, R., Schulze, E. D., Valentini, R., and Dolman, A. J.: Europe's terrestrial biosphere absorbs 7 to 12% ofeuropean anthropogenic CO2 emissions, Science, 300, 1538–1542, 2003

Kalbitz, K., Schmerwitz, J., Schwesig, D., and Matzner, E.: Biodegradation of soil-derived dissolved organic matter as related to its properties, Geoderma, 113, 273–291, 2003.
Kicklighter DW, et al. (2013) Insights and issues with simulating terrestrial DOC loading of Arctic river networks. Ecol Appl 23(8):1817–1836.

Kindler, R., Siemens, J., Kaiser, K., Walmsley, D. C., Bernhofer, C., Buchmann, N., Cellier, P., Eugster, W., Gleixner, G., Grunwald, T., Heim, A., Ibrom, A., Jones, S. K., Jones, M., Klumpp, K., Kutsch, W., Larsen, K. S., Lehuger, S., Loubet, B., Mckenzie, R., Moors, E., Osborne, B., Pilegaard, K., Rebmann, C., Saunders, M., Schmidt, M. W. I., Schrumpf, M., Seyfferth, J., Skiba, U., Soussana, J.-F., Sutton, M. A., Tefs, C., Vowinckel, B., Zeeman, M. J., and Kaupenjohann, M. Dissolved carbon leaching from soil is a crucial component of the net ecosystem carbon balance, Glob. Change Biol., 17, 1167–1185, https://doi.org/10.1111/j.1365-486.2010.02282.x, 2011.

Köchy, M., Hiederer, R., & Freibauer, a. (2015). Global distribution of soil organic carbon – Part 1: Masses and frequency distributions of SOC stocks for the tropics, permafrost regions, wetlands, and the world. *Soil*, *1*(1), 351–365. https://doi.org/10.5194/soil-1-351-2015.

Kramer K, Leinonen I, Bartelink HH et al. (2002) Evaluation of six process-based for- est growth models using eddy-covariance measurements of CO(2) and H(2)O fluxes at six forest sites in Europe. Global Change Biology, 8, 213–230.

Krinner, G. et al. A dynamic global vegetation model for studies of the coupled atmosphere-biosphere system. Global Biogeochem. Cycles 19, 1–33 (2005).

Lauerwald, R., Hartmann, J., Ludwig, W. & Moosdorf, N. Assessing the nonconservative fluvial fluxes of dissolved organic carbon in North America. *J. Geophys. Res.* **117**, G01027 (2012).

Lauerwald, R., Laruelle, G. G., Hartmann, J., Ciais, P., & Regnier, P. A. G. (2015). Spatial patterns in CO2 evasion from the global river net- work. Global Biogeochemical Cycles, 29(5), 534–554. https://doi. org/10.1002/2014GB004941

Lauerwald, R., Regnier, P., Camino-Serrano, M., Guenet, B., Guimberteau, M., Ducharne, A., … Ciais, P. (2017). ORCHILEAK (revision 3875): a new model branch to simulate carbon transfers along the terrestrial--aquatic continuum of the Amazon basin. Geoscientific Model Development, 10(10), 3821–3859. https://doi.org/10.5194/gmd-10-3821-2017.

Lauerwald,R.,Regnier, P.,Guenet,B., Friedlingstein, P;Ciais, P: How simulations of the land carbon sink are biased by ignoring fluvial carbon transfers –A case study for the Amazon basin, Volume 3, Issue 2, 21 August 2020, Pages 226-236 https://doi.org/10.1016/j.oneear.2020.07.009

Lehner B, Verdin K, Jarvis A. 2008. New global hydrography derived from spaceborne elevation data. *EOS, Transactions of the American Geophysical Union* **89**: 93– 104.

Leifeld, J., & Menichetti, L. (2018). The underappreciated potential of peatlands in global climate change mitigation strategies /704/47/4113 /704/106/47 article. Nature Communications, 9(1). https://doi.org/10.1038/s41467-018-03406-6

Le Quéré, C., Moriarty, R., Andrew, R. M., Peters, G. P., Ciais, P., Friedlingstein, P., Jones, S. D., Sitch, S., Tans, P., Arneth, A., Boden, T. A., Bopp, L., Bozec, Y., Canadell, J. G., Chini, L. P., Chevallier, F., Cosca, C. E., Harris, I., Hoppema, M., Houghton, R. A., House, J. I., Jain, A. K., Johannessen, T., Kato, E., Keel- ing, R. F., Kitidis, V., Klein Goldewijk, K., Koven, C., Landa, C. S., Landschützer, P., Lenton, A., Lima, I. D., Marland, G., Mathis, J. T., Metzl, N., Nojiri, Y., Olsen, A., Ono, T., Peng, S., Peters,W., Pfeil, B., Poulter, B., Raupach, M. R., Regnier, P., Rö- denbeck, C., Saito, S., Salisbury, J. E., Schuster, U., Schwinger, J., Séférian, R., Segschneider, J., Steinhoff, T., Stocker, B. D., Sutton, A. J., Takahashi, T., Tilbrook, B., van der Werf, G. R., Viovy, N.,Wang, Y.-P.,Wanninkhof, R.,Wiltshire, A., and Zeng, N.: Global carbon budget 2014, Earth Syst. Sci. Data, 7, 47–85, https://doi.org/10.5194/essd-7-47-2015, 2015.

Le Quéré, C., Andrew, R. M., Friedlingstein, P., Sitch, S., Pongratz, J., Manning, A. C., Korsbakken, J. I., Peters, G. P., Canadell, J. G., Jackson, R. B., Boden, T. A., Tans, P. P., Andrews, O. D., Arora, V. K., Bakker, D. C. E., Barbero, L., Becker, M., Betts, R. A., Bopp, L., Chevallier, F., Chini, L. P., Ciais, P., Cosca, C. E., Cross, J., Currie, K., Gasser, T., Harris, I., Hauck, J., Haverd, V., Houghton, R. A., Hunt, C. W., Hurtt, G., Ilyina, T., Jain, A. K., Kato, E., Kautz, M., Keeling, R. F., Klein Goldewijk, K., Körtzinger, A., Landschützer, P., Lefèvre, N., Lenton, A., Lienert, S., Lima, I., Lombardozzi, D., Metzl, N., Millero, F., Monteiro, P. M. S., Munro, D. R., Nabel, J. E. M. S., Nakaoka, S., Nojiri, Y., Padin, X. A., Peregon, A., Pfeil, B., Pierrot, D., Poulter, B., Rehder, G., Reimer, J., Rödenbeck, C., Schwinger, J., Séférian, R., Skjelvan, I., Stocker, B. D., Tian, H., Tilbrook, B., Tubiello, F. N., van der Laan-Luijkx, I. T., van der Werf, G. R., van

Heuven, S., Viovy, N., Vuichard, N., Walker, A. P., Watson, A. J., Wiltshire, A. J., Zaehle, S., and Zhu, D.: Global Carbon
870   Budget 2017, Earth Syst. Sci. Data, 10, 405–448, https://doi.org/10.5194/essd-10-405-2018, 2018.

Li, M., Peng, C., Zhou, X., Yang, Y., Guo, Y., Shi, G., & Zhu, Q. (2019). Modeling global riverine DOC flux
dynamics from 1951 to 2015. Journal of Advances in Modeling Earth Systems, 11, 514–530.
https://doi.org/10.1002/2018MS001363
875

Maavara, T., Lauerwald, R., Regnier, P., & Van Cappellen, P. (2017). Global perturbation of organic carbon cycling by river
damming. Nature Communications, 8(May), 1–10. https://doi.org/10.1038/ncomms15347

Mattsson T., P. Kortelainen, A. Laubel, D. Evans, M. Pujo-Pay, A. Raeike, P. Conan. Export of dissolved organic matter in
880   relation to land use along a European climatic gradient. Sci. Total Environ., 407 (2009), pp. 1967-1976

Michalzik B., Kalbitz K., Park J.H. and Matzner E. 2001. Fluxes and concentrations of dissolved organic carbon and
nitrogen – a synthesis for temperate forests. Biogeochemistry 52: 173–205

885   Nakhavali, M., Friedlingstein, P., Lauerwald, R., Tang, J., Chadburn, S., Camino-Serrano, M., Guenet, B., Harper, A.,
Walmsley, D., Peichl, M., and Gielen, B.: Representation of dissolved organic carbon in the JULES land surface model
(vn4.4_JULES-DOCM), Geosci. Model Dev., 11, 593–609, https://doi.org/10.5194/gmd-11-593-2018, 2018.

Nakhavali, M., Lauerwald, R., Regnier, P., Guenet, B., Chadburn, S., & Friedlingstein, P. (2021). Leaching of dissolved
890   organic carbon from mineral soils plays a significant role in the terrestrial carbon balance, (June 2020), 1083–1096.
https://doi.org/10.1111/gcb.15460.

Nash, J. E. and Sutcliffe, J. V.: River flow forecasting through con-ceptual models, Part I - A discussion of principles, J.
Hydrol., 10,282–290, 1970.
895

Neff J.C. and Asner G.P. 2001. Dissolved organic carbon in terrestrial ecosystems: a synthesis and a model. Ecosystems 4:
29–48.

d'Orgeval, T., Polcher, J., & de Rosnay, P. (2008). Sensitivity of the West African hydrological cycle in ORCHIDEE to
900   infiltration processes. Hydrology and Earth System Sciences, 12, 1387– 1401. https://doi.org/10.5194/hess-12-1387-2008
791

Parton, W. J., Stewart, J. W., and Cole, C. V.: Dynamics of C, N, P and S in grassland soils: a model, Biogeochemistry, 5,
109–131, https://doi.org/10.1007/bf02180320, 1988.
905

M. C. Peel, B. L. Finlayson, T. A. Mcmahon. Updated world map of the Köppen-Geiger climate classification. *Hydrology
and Earth System Sciences Discussions*, European Geosciences Union, 2007, 4 (2), pp.439-473. ⟨hal-00298818⟩

Peng, S., Ciais, P., Maignan, F., Li, W., Chang, J., Wang, T., and Yue, C.: Sensitivity of land use change emission estimates
910   to historical land use and land cover mapping, Global Biogeochem. Cy., 31, 626–643,
https://doi.org/10.1002/2015GB005360, 2017.

Polcher, J.: Les processus de surface à l'échelle globale et leurs interactions avec l'atmosphère, Habilitation à diriger des recherches, University Pierre et Marie Curie, Paris, France, 2003.

915

Raymond PA, Saiers JE (2010) Event controlled DOC export from forested watersheds. Biogeochemistry 100(1–3):197–209

Regnier, P., Friedlingstein, P., Ciais, P., Mackenzie, F. T., Gruber, N., Janssens, I. A., Laruelle, G. G., Lauerwald, R., Luyssaert, S., Andersson, A. J., Arndt, S., Arnosti, C., Borges, A. V., Dale, A. W., Gallego-Sala, A., Goddéris, Y., Goossens,
920   N., Hartmann, J., Heinze, C., Ilyina, T., Joos, F., Larowe, D. E., Leifeld, J., Meysman, F. J. R., Munhoven, G., Raymond, P. A., Spahni, R., Suntharalingam, P., and Thullner, M.: Anthropogenic perturba- tion of the carbon fluxes from land to ocean, Nat. Geosci., 6, 597–607, https://doi.org/10.1038/ngeo1830, 2013.

Reynolds, C., Jackson, T. & Rawls, W. Estimating available water content by linking 424 the FAO soil map of the world
925   with global soil profile databases and pedo-transfer 425 functions. Am. Geophys. Union Fall Meet. EOS Trans. Spring Meet. Suppl. 80, S132 426 (1999).

de Rosnay, P., Polcher, J., Bruen, M., and Laval, K.: Im- pact of a physically based soil water flow and soil- plant interaction representation for modeling large-scale land surface processes, J. Geophys. Res.-Atmos., 107, 4118,
930   https://doi.org/10.1029/2001JD000634, 2002.

Saxton KE, Rawls WJ, Romberger SJ, Papendick RI (1986) Estimating generalized soil-water characteristics from texture. Soil Science Society of America Journal, 50, 1031–1036.

935   Sitch, S. et al. (2003), Evaluation of ecosystem dynamics, plant geography and terrestrial carbon cycling in the LPJ dynamic global vegetation model, Glob. Chang. Biol., 9(2), 161–185, doi:10.1046/j.1365-2486.2003.00569.x.

Smith, J., Gottschalk, P., Bellarby, J., Chapman, S., Lilly, A., Tow- ers, W., Bell, J., Coleman, K., Nayak, D., Richards, M., Hillier, J., Flynn, H., Wattenbach, M., Aitkenhead, M., Yeluripurti, J., Farmer, J., Milne, R., Thomson, A., Evans, C., and
940   Smith, P.: Estimating changes in national soil carbon stocks using ECOSSE – a new model that includes upland organic soils. Part II. Application in Scotland, Clim. Res., 45, 193–205, https://doi.org/10.3354/cr00902, 2010.

Sun, Y., Goll, D. S., Chang, J., Ciais, P., Guenet, B., Helfenstein, J., Huang, Y., Lauerwald, R., Maignan, F., Naipal, V., Wang, Y., Yang, H., and Zhang, H.: Global evaluation of the nutrient-enabled version of the land surface model
945   ORCHIDEE-CNP v1.2 (r5986), Geosci. Model Dev., 14, 1987–2010, https://doi.org/10.5194/gmd-14-1987-2021, 2021.

Tian, H., Q. Yang, R. G. Najjar, W. Ren, M. A. M. Friedrichs, C. S. Hopkinson, and S. Pan (2015), Anthropogenic and climatic influences on carbon fluxes from eastern North America to the Atlantic Ocean: A process-based modeling study, J. Geophys. Res. Biogeosci., 120, 752–772, doi:10.1002/ 2014JG002760.

950

Turgeon, J.: Production and biodegradation of dissolved carbon, nitrogen and phosphorus from Canadian forest floors, McGill University, 2008.

Turner D.P., W.D. Ritts, W.B. Cohen, S.T. Gower, S.W. Running, M. Zhao, M.H. Costa, A.A. Kirschbaum, J.M. Ham, S.R.

955   Saleska, D.E. Ahl. Evaluation of MODIS NPP and GPP products across multiple biomes. Remote Sens. Environ., 102 (3-4)

(2006), pp. 282-292, 10.1016/j.rse.2006.02.017

Vorosmarty, C. J., B. M. Fekete, M. Meybeck, and R. B. Lammers, Geo- morphometric attributes of the global system of

rivers at 30-minute spa- tial resolution, J. Hydrol., 237, 17–39, 2000.

960

Vuichard et al., 2018, Accounting for Carbon and Nitrogen interactions in the Global Terrestrial Ecosystem Model

ORCHIDEE (trunk version, rev 4999): multi-scale evaluation of gross primary production. Geosci. Model Dev. Discuss.,

https://doi.org/10.5194/gmd-2018-261

965   Weedon, G. P., G. Balsamo, N. Bellouin, S. Gomes, M. J. Best, and P. Viterbo (2014), The WFDEI meteorological forcing

data set: WATCH Forcing Data methodology applied to ERA-Interim reanalysis data, Water Resour. Res., 50, 7505–7514,

doi:10.1002/2014WR015638.

Worrall, F., and T. P. Burt (2007), Flux of dissolved organic carbon from U.K. rivers, Global Biogeochem. Cycles, 21,

970   GB1013, doi:10.1029/2006GB002709.

Worrall F. , Davies H., Bhogal A., Lilly A., Evans M.G. , Turner K., Burt T.P., Barraclough D. , Smith P. , Merrington

G. The flux of DOC from the UK – predicting the role of soils, land use and in-stream losses. J. Hydrol., 448–449 (2012),

pp. 149-160

975

Zhang, B., Tian, H., Lu, C., Dangal, S. R. S., Yang, J., and Pan, S.: Global manure nitrogen production and application in

cropland during 1860–2014: a 5 arcmin gridded global dataset for Earth system modeling, Earth Syst. Sci. Data, 9, 667–678,

https://doi.org/10.5194/essd-9-667-2017, 2017.

980   Zhao, M., F. A. Heinsch, R. R. Nemani, and S. W. Running (2005), Improvements of the MODIS terrestrial gross and net

primary production global data set, Remote Sens. Environ., 95(2), 164–176, doi:10.1016/j.rse.2004.12.011.